STUDENT POSTERS

NUCLEAR DAYS 2022

Pilsen, Czech Republic

www.jadernedny.cz

Poster Scientific Committee

doc. Ing. František HEZOUČKÝ, Ph.D.	University of West Bohemia
RNDr. Miroslav KAWALEC	Czech Nuclear Society
Ing. Karel BÍŽA	ÚJV Řež, a. s.

Organizing Committee

Ing. Jan ZDEBOR, CSc.	University of West Bohemia
Ing. Michal VOLF	University of West Bohemia
Ing. Jana JIŘIČKOVÁ, Ph.D.	University of West Bohemia
Mgr. Eva KOREISOVÁ	University of West Bohemia
Michaela VACKOVÁ	University of West Bohemia
Lucie GRUSOVÁ	ŠKODA JS a.s.

Partners of Nuclear Days 2022

General partner

ŠKODA JS

Platinum partner

KHNP
KOREA HYDRO & NUCLEAR POWER CO., LTD

Gold partners

ÚJV

MVM EGI

fortum

DOOSAN
Škoda Power

javys

Westinghouse

Silver partners

Media partners

Content

BACHELOR STUDENTS

SMALL MODULAR REACTORS AND THEIR POSSIBLE APPLICATION IN THE ENERGY INDUSTRY OF THE CZECH REPUBLIC

Marek HOLEČEK

Czech Technical University in Prague, Faculty of Electrical Engineering, Prague, Czech Republic

A small modular reactor is defined as a nuclear reactor up to an electrical power of 300 MWe. This special type of reactor is composed of individual modules that are manufactured in a factory and brought as a unit to the construction site for faster assembly. It is a most advanced type of reactor that largely complies with passive safety, i.e. the use of as few active parts as possible in the reactor and the use of physical principles such as gravity, pressure differential or natural flow and conduction. In addition to passive safety, depth protection is used to ensure that in the event of a reactor accident, the immediate surroundings are not endangered. Small modular reactors often also use an integral primary circuit arrangement. This means that the nuclear fuel, control rods, circulation pumps and steam generators are all contained in a single pressure vessel.

Small Modular Reactors

and their possible application in the energy industry of the Czech Republic

Marek Holeček, CTU FEL

Introduction

A small modular reactor is defined as a nuclear reactor up to an electrical power of 300 MWe. This special type of reactor is composed of individual modules that are manufactured in a factory and brought as a unit to the construction site for faster assembly. It is a most advanced type of reactor that largely complies with passive safety, i.e. the use of as few active parts as possible in the reactor and the use of physical principles such as gravity, pressure differential or natural flow and conduction. In addition to passive safety, depth protection is used to ensure that in the event of a reactor accident, the immediate surroundings are not endangered. Small modular reactors often also use an integral primary circuit arrangement. This means that the nuclear fuel, control rods, circulation pumps and steam generators are all contained in a single pressure vessel.

The main advantage of SMR

The main advantage of the small modular reactor concept is its lower cost. The lower price is associated with lower risk for investors, and it is therefore expected that investors will prefer this form of investment to conventional nuclear power plants. For some SMR variants, the investment can be spread over more modules, and as a result, modules can also provide comparable power to a conventional plant without as much risk and with faster construction. At the same time, it is important to remember that a lower price does not mean a lower price per unit of energy, the price per unit is higher, and that the main part is still fixed costs.

Figure 1. NuScale reactor building

	Name of the Project					
Parameter	SMART	NuScale	UK SMR	SMR160	BWRX300	NUWARD
Type of reactor	iPWR	iPWR	PWR	PWR	BWR	iPWR
P_{inst} – therm [MWt]	365	200/module	1276	525	870	2 x 540
P_{inst} – el [MWe]	107	60/module	470	160	270-290	2 x 170
Lifespan [years]	60	60	60	80	60	60

Table 1. SMR variants considered for the Czech republic by ČEZ

Suitable SMR types

All the concepts under consideration are light water reactors, most of them of the pressurized water integral type. The main parameters of the variants considered for use in the Czech Republic according to ČEZ are indicated in Table 1. SMART is a South Korean project, NuScale, BWRX300 and SMR160 from the USA, UK SMR from the UK and NUWARD from France. The NuScale reactor can be modularized with up to 12 modules. This table is final, so it is likely that one of the named will be used in the Czech Republic. Standard uranium oxide, enriched up to 5%, is used as fuel for all considered variants.

Suitable applications for SMR

In the Czech Republic, SMRs could serve alongside renewable energy sources or as a replacement for conventional power plants. However, SMR projects are still untested, so it is not certain that they will be sufficiently flexible. They could also act as ancillary services or as heat supply instead of conventional thermal plants. Their location would allow heat to be transferred over shorter distances with significantly lower losses. In the near future, however, it is still preferable not to replace conventional NPPs and to use SMRs only as a supplement.

By 2030, coal is to be fully replaced and gas seems to be the only option. It could then be fully replaced by SMR and carbon neutrality would be ensured by 2050. Replacing thermal sources as opposed to electric seems a bit more realistic. There is not the amount of reactors needed to replace the thermal output of thermal plants with SMRs as would be needed if conventional coal plants were replaced. Small modular reactors, like nuclear power sources, would be able to deliver stable power output and the associated stable price of electricity or thermal energy. Thus, this price can easily be taken into account and predicted. In the future, some concepts envisage hydrogen production.

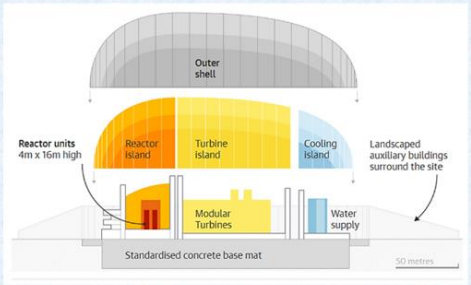

Figure 2. UK SMR reactor building

Conclusions

Given the reduction of emission sources and the great potential of nuclear power in the Czech Republic, the question of using small modular reactors is quite appropriate. As non-emission sources, they would be a suitable candidate to replace current coal or gas-fired power plants. With the rising price of emission allowances, oil and gas, the use of nuclear sources seems to be economically viable.

The use of nuclear power could be an option to ensure carbon neutrality and reduce the release of CO2 and other harmful gases into the atmosphere. Renewable sources suffer from uneven power delivery and so cannot operate without any stabilizing power source on the grid. And that source could be a small modular reactor.

The obstacle to this idea in the Czech Republic is their unpreparedness. However, according to the planned projects in the world and in our country, it is expected that this technology will take hold and will be more widespread and therefore cheaper. The first modular reactors will be of the tested light-water type, which is also reflected in the selection of variants in Table 1.

Small modular reactors are also an opportunity to keep nuclear know-how in the Czech Republic and to involve the Czech industry in this sector in the global market. When selecting the SMR option for the Czech Republic, this is considered. From the point of view of the state, this would possibly be another future money income for the state. On the other hand, this is not a priority; the primary objective of the SMR is to provide energy needs at the lowest possible cost. At the same time, this could lead to the development of technology and technically oriented students in this sphere.

References

1. ČERNÝ, Viktor. ČEZ – Malé modulární jaderné reaktory v ČR [presentation]. Praha: ČEZ, 2022 [cit. 2022-03-15].
2. ČEZ. Malé modulární reaktory SMR [presentation]. Elektrárna Temelín II, 2022 [cit. 2022-04-27].
3. NEA, 2021. Small Modular Reactors: Challenges and Opportunities [online]. [cit. 2022-05-07].
4. NUSCALE POWER. NuScale Power Reactor Building [online]. NuScale Power [cit. 2022-04-20].
5. ROLLS ROYCE. Rolls Royce Plant [online]. Rolls Royce [cit. 2022-04-22]
6. WORLD NUCLEAR ASSOCIATION. Small Nuclear Power Reactors [online]. 2021 [cit. 2022-04-21].

ANALYSIS OF OPERATIONAL CHARACTERISTICS OF A SMR WITH ATF

Ondřej LACHOUT, Pavel SUK

Faculty of Nuclear Sciences and Physical Engineering, Czech Technical University in Prague, Prague, Czech Republic

The behaviour of ATFs (Accident Tolerant Fuel) in large cores has already been investigated in depth, but analyses of ATF fuels in a SMR (Small Modular Reactor) core have not yet been studied in more detail. For this purpose, a 3D full-core calculation for the SMR designed by NuScale Power company was performed using the deterministic macrocode PARCS. The neutronic behaviour of selected ATF fuel candidates was analysed in this model.

Analysis of Operational Characteristics of a SMR with ATF

Ondřej Lachout (Author), Ing. Pavel Suk (Co-author)

lachoond@fjfi.cvut.cz
Faculty of Nuclear Sciences and Physical Engineering
Czech Technical University in Prague

ABSTRACT

The behaviour of ATFs (Accident Tolerant Fuel) in large cores has already been investigated in depth, but analyses of ATF fuels in a SMR (Small Modular Reactor) core have not yet been studied in more detail. For this purpose, a 3D full-core calculation for the SMR designed by NuScale Power company was performed using the deterministic macrocode PARCS. The neutronic behaviour of selected ATF fuel candidates was analysed in this model.

FULL-CORE CALCULATIONS

Full-core calculations for nuclear reactors are performed for safety reports and optimization of the fuel core loading. Regarding high calculation time-dependence, less demanding deterministic macrocodes are used for providing full-core calculations. Deterministic macrocode PARCS was chosen for full-core neutronic analysis. The main advantage of PARCS is the possibility to be coupled with external thermo-hydraulic or thermomechanical codes like TRACE and RELAP5. The process of macroscopic data preparation and deterministic full-core calculation cycle is visualized in Fig. 2. [1]

NUSCALE SMR

Nowadays the worldwide initiative is to divest from high emission energy sources. Therefore, many fossil fuel power plants are being closed all over the world at the moment. The arising problem is that those closed power plants have to be somehow replaced by a "clean", reliable, safe and high-efficiency energy source. The solution for this problem seems to be SMRs. There are many concepts of SMRs, but the most advanced one appears to be SMR by the NuScale Power company. NuScale's reactor is a light-water reactor with a thermal output of 160 MWt. One module includes the whole primary circuit as presented in Fig. 1. Concepts are count with 6 or 12 modules per a power plant. Basic technical data of one module of the NuScale reactor are summarized in Tab. 1. [2]

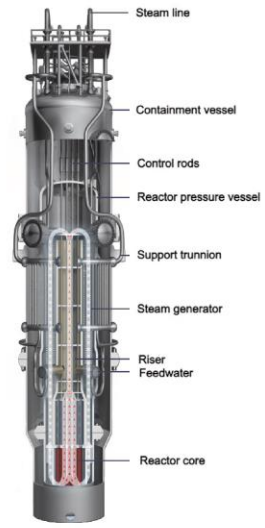

Figure 1: *NuScale module visualisation [2] (modified)*

Parameter	Value
Thermal power (MWt)	160
Electrical power (MWe)	77
Primary coolant pressure (MPa)	12.76
Average core temperature (°C)	284
Core diametr (cm)	151
Number of fuel assemblies (-)	37
Number of fuel pins per assembly (-)	264
Fuel enrichment - UO_2 (wt.%)	<5
Fuel cladding (-)	M5
Concentration of burnable absorber - Gd_2O_3 (wt.%)	<8

Table 1: *Basic technical data of NuScale SMR [3]*

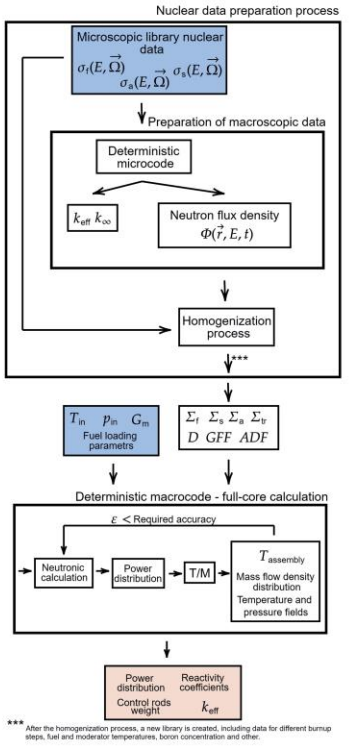

Figure 2: *Scheme of macroscopic data preparation and deterministic full-core calculation cycle*

CALCULATIONS

The full-core calculation, for the NuScale reactor, was performed on an existing model in deterministic macrocode PARCS. Nuclear macroscopic data were prepared for chosen ATF concepts. Analysed combination of fuel pellets and claddings were:

- UO_2 - M5,
- UN - M5,
- UO_2-10BeO - APMT+Tyranno SA3 (inner cladding thickness 0.55 mm consisting of Tyranno SA3 composition and an outer cladding 0.0596 mm thickness consisting of APMT).

Isotopic composition and densities of analysed fuel concepts are summarized in Tab. 2.

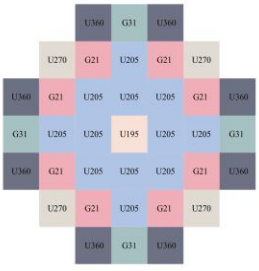

Figure 3: *Scheme of NuScale AZ model*

U195 – 1.95% uniformly enriched fuel pins,
U205 – 2.05% uniformly enriched fuel pins,
U270 – 2.70% uniformly enriched fuel pins,
U360 – 3.60% uniformly enriched fuel pins,
G21 – 256 fuel pins enriched to 2.70%, 8 pins enriched to 1.8% with 2.5% of Gd absorber,
G31 - 256 fuel pins enriched to 3.60%, 8 pins enriched to 1.5% with 3.0% of Gd absorber.

	Isotopic composition (wt.%)	Density (g/cm^3)
M5	98.86Zr-1.0Nb-0.14O	6.54
APMT	70.08Fe-22Cr-5Al-0.47Si-2.45Mo	7.49
Tyranno SA3	68.8Si-31C-0.2O	3.10
UO_2	88.1U-11.9O	10.96
UN	94.4U-5.6N (94.1 % ^{15}N)	14.33
UO_2-10BeO	79.3U-3.6Be-17.1O	9.68

Table 2: *Isotopic composition and densities of analysed fuel concepts [4]*

Critical Boron Concentration

Critical boron concentration (BC) was analysed for fully extended control and maximal reactor power. The fuel was burned for 720 days with 10 days step. In each step, the critical BC was calculated.
Fig. 4 shows the dependence of critical boron concentration on burnup time for all selected combinations of pellets and claddings. For UO_2-10BeO - APMT+Tyranno SA3 combination the critical BC decreases to zero around 620 burnup day. After this day critical state cannot be achieved.

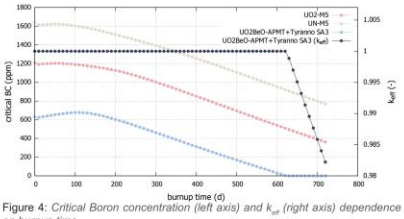

Figure 4: *Critical Boron concentration (left axis) and k_{eff} (right axis) dependence on burnup time*

Control Rods Weight

Control rods (CR) weights were analysed for all 4 groups included in NuScale´s reactor design. The position of each CR group is shown in Fig. 5. Results of CR weights for each group and analysed fuel concepts are presented in Fig. 6.

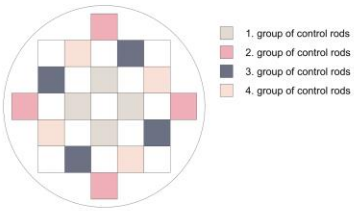

Figure 5: *Positions of different groups of control rods in AZ of NuScale reacotor*

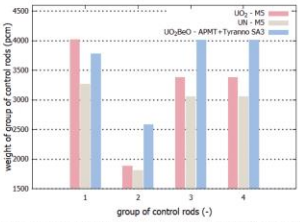

Figure 6: *Weight of each group of control rods for different fuel types*

Power Distribution

Power distrbution is visualized in Fig. 7 at the beginning of fuel burnup for NuScale's design-bases fuel combination (UO_2-M5). Fig. 8 shows a model of an analysed infinite fuel assembly.

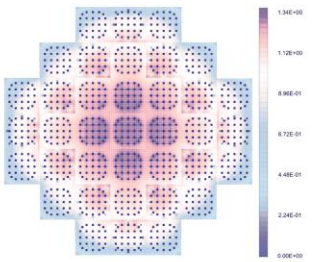

Figure 7: *Power distribution in NuScale core (UO_2-M5)*

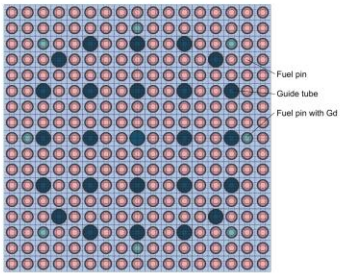

Figure 8: *Model of infinite fuel assembly*

Reactivity Coefficients

Reactivity coefficients were analysed for two cases:
- reactor power increase (Fig. 9),
- inlet moderator temperature increase (Fig. 10).

Reactivity changes for both cases are shown for an increase of 1 % power, respectively 1 K.
Fig. 10 shows, that with inlet moderator temperature increase the reactivity of the UO_2-10BeO - APMT+Tyranno SA3 rises. This effect is most likely to occur due to an over-moderated system. Solving this undesirable effect would require a change of fuel lattice geometry and further detailed analysis.

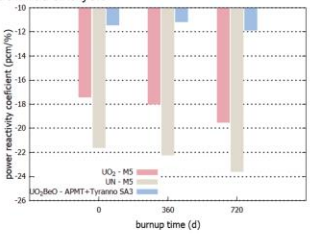

Figure 9: *Power reactivity coefficient in 3 burnups for different fuel types*

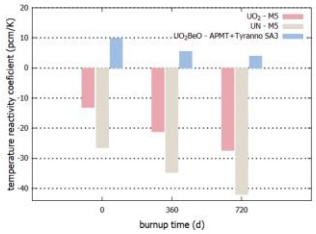

Figure 10: *Temperature reactivity coefficient in 3 burnups for different fuel types*

CONCLUSION

Neutronic analysis for a wider range of ATF concepts was performed on an infinite fuel assembly model in deterministic macrocode SCALE-TRITON. Results from this analysis agree with results from the full-core model. Furthermore, these analysis shows minimal neutronic changes when different fuel claddings types are used.
From performed calculations of NuScale's core model follows positive reactivity coefficients for inlet temperature rise for UO_2-10BeO pellet. Based on this analyse UO_2-10BeO pellet does not appear to be a suitable ATF concept for SMR.
On the other hand, ATF fuel pellet UN shows better behaviour in undesirable reactor conditions than conventional UO_2.

REFERENCES

[1] A. Ward, Y. Xu and T. Downar, Code for Generating the PARCS Cross Section, University of Michigan, http://nuram.engin.umich.edu/software/genpmaxs/, 2016.
[2] P.Suk, et al., Simulation of a NuScale core design with the CASL VERA code, Nuclear Engineering and Design, https://doi.org/10.1016/j.nucengdes.2020.110956, 2021.
[3] NuScale Power LLC, NuScale Standard Plant Design Certification Application - Chapter Four Reactor, https://www.nrc.gov/docs/ML2003/ML20036D438.pdf, 2020.
[4] Nuclear Energy Agency, State-of-the-Art Report on Light Water Reactor Accident-Tolerant Fuels, https://www.oecdilibrary.org/content/publication/9789264308343-en, 2018.

NUCLEAR REACTORS FOR SPACE EXPLORATION

Josef SABOL

Faculty of Nuclear Sciences and Physical Engineering, Czech Technical University in Prague, Prague, Czech Republic

Space nuclear reactors were very important in space exploration in the 20th century. Thanks to their power, they made it possible to use satellites with higher power requirements in space. This aspect was mainly relevant to the USSRs, which launched 33 satellites powered by nuclear reactors in the period between the years 1970 and 1988. In contrast the USA sending only one. Radioisotope sources have been and continue to be used in space, generating heat due to the decay of ^{238}Pu. However, this poster only deals with nuclear reactors used or planned for space exploration.

NUCLEAR REACTORS FOR SPACE EXPLORATION

JOSEF SABOL
saboljos@fjfi.cvut.cz

Faculty of Nuclear Sciences and Physical Engineering
Czech Technical University in Prague

INTRODUCTION

Space nuclear reactors were very important in space exploration in the 20th century. Thanks to their power, they made it possible to use satellites with higher power requirements in space. This aspect was mainly relevant to the USSRs, which launched 33 satellites powered by nuclear reactors in the period between the years 1970 and 1988. In contrast the USA sending only one.

Radioisotope sources have been and continue to be used in space, generating heat due to the decay of ^{238}Pu. However, this poster only deals with nuclear reactors used or planned for space exploration [1].

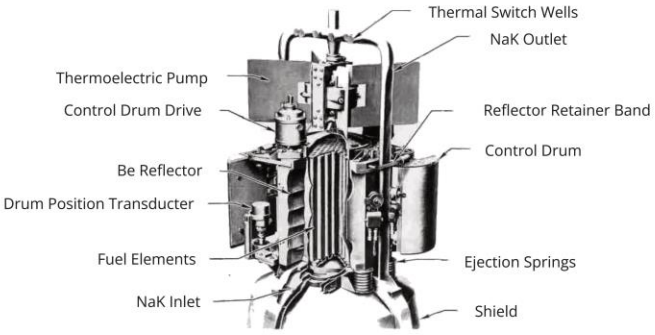

Figure 1: Cross section view of SNAP-10A reactor.

1. NUCLEAR REACTOR SNAP-10A

The SNAP-10A was a thermal nuclear reactor used once in 1965 by the USA. It reached a heat output of 35 kW and used thermoelectric cells to convert it into electricity with an output of ca. 550 W.

It used U-ZrH pellets with 93% enrichment arranged in fuel rods and covered with Hastelloy (nickel-based alloy) as fuel.

It was cooled with a eutectic alloy consisting of liquid Na and K (NaK-78) with an outlet temperature of 560 °C. Beryllium control drums around the core served for reactivity control via neutron reflection. The shielding consisted of stainless steel with LiH [2].

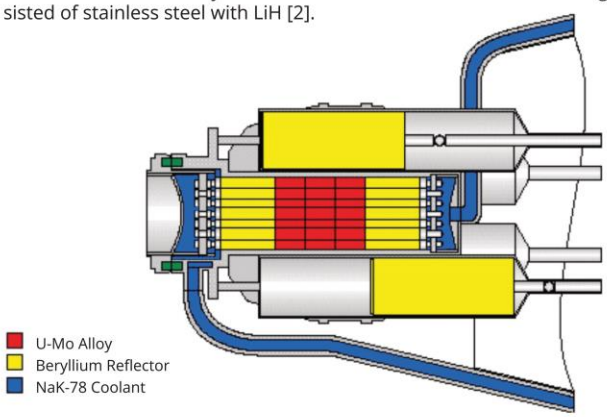

Figure 2: Drawing of BES-5 reactor.

2. NUCLEAR REACTOR BES-5

The BES-5 was a fast reactor used by the USSRs between the years 1970 and 1988 in 31 space missions. It reached a heat output of 100 kW, which was converted into electricity with a power output of 3 kW by thermoelectric cells.

It used U-Mo alloy with 90% uranium enrichment as fuel. The core consisted of 37 fuel rods coated by stainless steel. Axial beryllium reflectors were placed at each end piece.

Six cylindrical beryllium reflectors around the vessel were used to regulate the power by controlling the reactivity via neutron reflection. NaK-78 alloy served as a coolant at an operating temperature of 700 °C. The shielding consisted of stainless steel with LiH [2].

3. OTHER PROJECTS

In the 1970s, the USSR developed two new and more powerful reactors: **TOPAZ-I** and **TOPAZ-II.** In 1987 only two TOPAZ-I models were launched. No reactor has entered space since then [2].

In the USA, several other projects have emerged after the SNAP-10A reactor, namely: **SP-100, SAFE-400, HOMER-15**, and the most recent **KRUSTY** reactor [3].

4. NUCLEAR REACTOR KRUSTY

KRUSTY is a prototype experimental high-speed reactor built and tested between the years 2015–2018 under the KiloPower program (a program that develops a reactor up to 10 kW electrical) in the USA.

It achieved a heat output of 4 kW, which was converted into electricity with an output of 1 kW using 8 heat pipes and Stirling motors. It used a U-Mo block with 93% uranium enrichment as fuel. It also contained a reflector made of BeO, a shield made of stainless steel and a control rod made of B_4C. More information about the reactor and its testing can be found in [4].

An extraordinary thing about the reactor was the method of safety shutdown. The vessel was surrounded by a radial reflector which could be moved in the axial direction. Depending on the position of the control rod and the gap between radial reflectors, the k_{eff} was calculated with the code Serpent 2.

Negative temperature reactivity coefficients are essential for a stable reactor operation. The fuel temperature reactivity coefficient for this reactor design was calculated as (−0.740 ± 0.136) ppm/K.

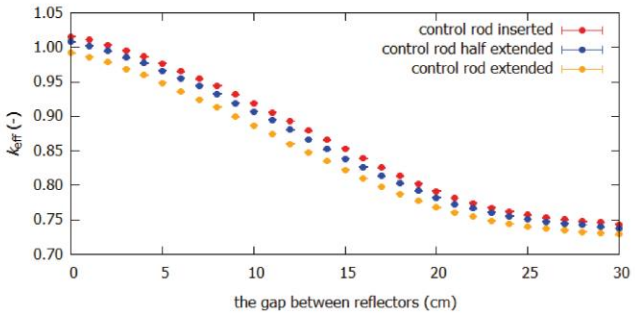

Figure 3: Dependence between k_{eff} and the gap between the radial reflectors at different positions of the control rod.

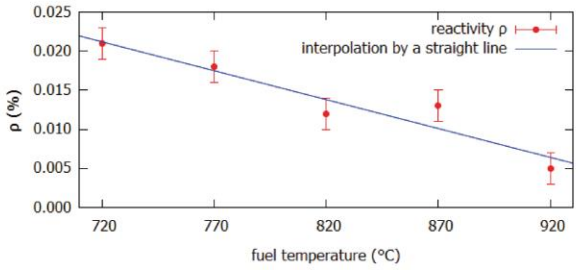

Figure 4: Dependence between ρ and fuel temperature.

CONCLUSION

The development of space nuclear reactors is essential for operation of power demanding instruments in space and on the planets where solar panels cannot be used. It is the only way to produce enough electricity for a more permanent stay on the Moon or for the way to Mars.

REFERENCES

[1] WAGNER, Vladimír. Jaderné zdroje pro vesmírnou kolonizaci. http://ojs.ujf.cas.cz/~wagner/popclan/sondy/jadernezdroje.html.
[2] EL-GENK, M. S. Deployment history and design considerations for space reactor power systems. Acta Astronautica. ISSN 0094-5765.
[3] Nuclear Reactors and Radioisotopes for Space. World Nuclear Asociation. https://world-nuclear.org/information-library/non-power-nuclearapplications/transport/nuclear-reactors-for-space.aspx
[4] POSTON, David I.; GIBSON, Marc A.; GODFROY Thomas a McCLURE, Patrick R. KRUSTY Reactor Design. Nuclear Technology. ISSN 0029-5450.

SMRs TECHNOLOGIES FOR DISTRICT HEATING IN THE CZECH REPUBLIC

Jan ULLMANN

Faculty of Electrical Engineering, University of West Bohemia, Pilsen, Czech Republic

The bachelor's thesis deals with analysing SMRs for heat production. It introduces several promising SMR concepts and analyses the heating system of the Czech Republic. The final part is devoted to comparing the given reactors for regional locations in the Czech Republic.

FACULTY OF ELECTRICAL ENGINEERING
UNIVERSITY OF WEST BOHEMIA

SMRs technologies for district heating in the Czech Republic

NUCLEAR DAYS

Author: Bc. Jan Ullmann, Bachelor thesis supervisor: Ing. Mašata

The bachelor´s thesis deals with analysing SMRs for heat production. It introduces several promising SMR concepts and analyses the heating system of the Czech Republic. The final part is devoted to comparing the given reactors for regional locations in the Czech Republic.

Small modular reactors

Small modular reactors are **nuclear reactors up to 300 MW(e)** with a safety zone radius of up to 300 meters. Modular means that the reactor is assembled in a compact box, the system is manufactured in series production and is only subsequently transported to the place of operation.

Overview of SMRs

Here is my overview of promising SMRs. The selection was based on power output and geographical diversification.

Reactor	MWt	MWe	Country of development	State of development
TEPLATOR	50	-	Czech Republic	Conceptual design
DHR400	400	-	China	2024 into operation
HAPPY200	200	-	China	2024 into operation
RUTA-70	70	-	Russia	Simulation
KLT-40 S	150	30	Russia	Commercial operation
SMART	365	107	Korea/SA	Design approved
BWRX-300	870	300	Japan	2027 into operation
ACP100	385	125	China	2026 into operation

Tab. 1: Overview of SMRs

The heating system of the Czech Republic

More than 1.5 million households are served by district heating. This fact is more common in the northern countries of Europe because they are experiencing a colder winter period than the Czech Republic.

The most used fuel in the energy mix of the Czech Republic is lignite (40%), followed by natural gas.

The biggest problem of the heating system is the price of emission allowances and the price of natural gas.

Of course, ecologization and decarbonisation are part of this issue, some coal sources have been converted to gas sources. A big topic is the reconstruction of steam heat distribution to reduce heat loss.

SMRs for heat production

This section contains a look at the **power regulation of nuclear sources**. Regulation of the nuclear source is undesirable from an economic point of view due to high investment costs. For my calculation, I take only reactors that operate without energy conversion. On the other hand, cogeneration production has the advantage of easy regulation during the year.

The first regulated production follows consumption during the heating season (based on comparative reports of the Energy Regulatory Office of the Czech Republic). Table 2 shows the regulation during the year and the heat supplied by the proposed reactors.

Reactor	Power (MWt)	Produced heat (TJ)				Total (TJ)
		2 months (100 %)	4 months (75 %)	2 months (50 %)	1 months (40 %)	
TEPLATOR	50	260	390	130	50	830
RUTA-70	70	360	550	180	70	1160
HAPPY200	200	1040	1560	520	210	3330
DHR400	400	2070	3110	1040	410	6630

Tab. 2: Demand-driven heat production

Second unregulated view assumes an average power load of 85% for 9 months (See Table 3). This approach is standard for nuclear sources.

Reactor	Power (MWt)	Produced heat (TJ)
		9 months (85 %)
TEPLATOR	50	990
RUTA-70	70	1390
HAPPY200	200	3970
DHR400	400	7930

Tab. 3: Unregulated heat production

Identification of suitable locations for a nuclear source

New location - evaluation of a new location using extensive **geological measurements**, there can be no occurrence of coal mining, which is a **big problem due to replacing outdated coal-fired power plants.**

The complex evaluation of a new location significantly exceeds the scope of my bachelor´s thesis.

=> Historically selected nuclear locations (**Tetov**, Opatovice nad Labem, **Blahutovice**)

=> Locations with a nuclear facility in operation (**Řež**, Temelín, Dukovany)

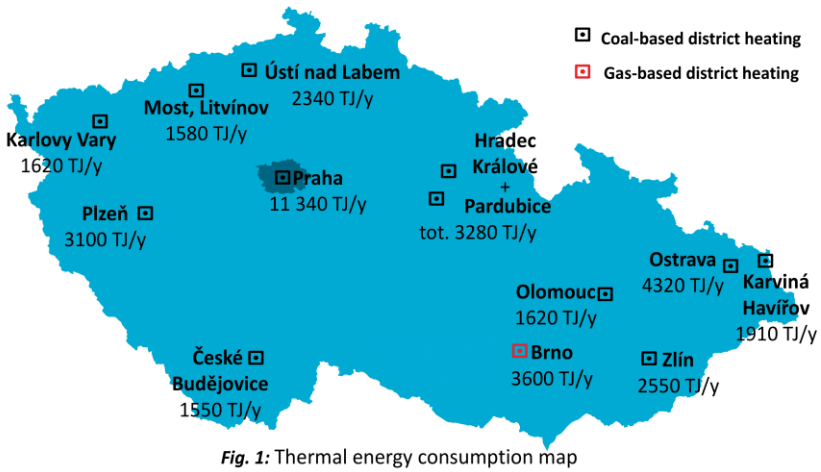

Fig. 1: Thermal energy consumption map

This evaluation is only based on the demand for supplied heat (See Table 3) and does not consider the requirements for nuclear source.

Based on performance diversification, we can choose any regional city and assign it to an individual reactor (See Fig. 1).

Results – proposed locations

Locations	Reactor type	Produced heat
Řež (Prague)	DHR400	7930 TJ/y
Blahutovice (Ostrava)	HAPPY200	3970 TJ/y
Tetov (Pardubice+Hr. Králové)	3x TEPLATOR	2970 TJ/y

Tab. 4: Proposed locations

Selection of all these variants is only based on the amount of produced heat, and supplemented with a gas source is required. **Considering power diversification, all reactors, especially with cogeneration, can be fitted to every regional city in the Czech Republic**.

Conclusion

Currently, proposed gas-fired power plants are a temporary solution -> SMRs may follow.

SMRs with cogeneration production can replace coal-fired power plants because of easier regulation and also represent zero-carbon heat production.

So far, no SMR has been approved and licensed in the Czech Republic.

These days, only one reactor, Akademik Lomonosov, is in commercial operation (See Table 1).

MASTER STUDENTS

HIGH TEMPERATURE BEHAVIOUR OF Cr-Ni CLADDING CONCEPT

A. CHALUPOVÁ[1,2], J. KREJČÍ[1], P. ČERVENKA[1,2], V. ROZKOŠNÝ[1], F. MANOCH[1], J. SÝKORA[1], M. ŠEVEČEK[2], P. HALODOVÁ[3], P. GÁVELOVÁ[3]

[1]UJP PRAHA a.s., Prague, Czech Republic

[2]Czech Technical University in Prague, Prague, Czech Republic

[3]Research Centre Řež s.r.o. Řež, Czech Republic

Zirconium fuel claddings are used in current light water reactors due to their many beneficial properties during normal operation. However, these materials present some limitations when operating conditions change to a design or even beyond the design accident scenario. The rapid exothermic oxidation between zirconium and water vapour at high temperatures degrades the system's coolability and, at the same time, generates a significant amount of hydrogen that deteriorates reactor safety. In recent decades, severe nuclear accidents have highlighted these difficulties and motivated the development of accident tolerant fuel. These fuels are entirely new and possibly modified types of nuclear fuels that can tolerate accident conditions in the reactor core for extended time periods and up to higher temperatures. The other goals of these fuels include increasing safety margins and achieving a higher operating economy.

The presented study investigates the behaviour of advanced cladding made of Cr-Ni alloy and a reference zirconium alloy during a hypothetical LB-LOCA light water reactor accident. A set of experiments aimed at determining the melting temperature, characterising the high-temperature oxidation kinetics, and the creep rate was carried out at UJP PRAHA a.s. and the Karlsruhe Institute of Technology.

High Temperature Behaviour of Cr-Ni Cladding Concept

A. Chalupová[1,2], J. Krejčí[1], P. Červenka[1,2], V. Rozkošný[1], F. Manoch[1], J. Sýkora[1], M. Ševeček[2], P. Halodová[3], P. Gávelová[3]

[1] UJP PRAHA a.s., [2] CTU in Prague, [3] Research Centre Řež

adela.chalupova@email.com

WHY DOES THIS MATTER?

Zirconium fuel claddings are used in current light water reactors due to their many beneficial properties during normal operation. However, these materials present some limitations when operating conditions change to a design or even beyond the design accident scenario. The rapid exothermic oxidation between zirconium and water vapour at high temperatures degrades the system's coolability and, at the same time, generates a significant amount of hydrogen that deteriorates reactor safety. In recent decades, severe nuclear accidents have highlighted these difficulties and motivated the development of accident tolerant fuel. These fuels are entirely new and possibly modified types of nuclear fuels that can tolerate accident conditions in the reactor core for extended time periods and up to higher temperatures. The other goals of these fuels include increasing safety margins and achieving a higher operating economy.

The presented study investigates the behaviour of advanced cladding made of Cr-Ni alloy and a reference zirconium alloy during a hypothetical LB-LOCA light water reactor accident [1]. A set of experiments aimed at determining the melting temperature, characterising the high-temperature oxidation kinetics, and the creep rate was carried out at UJP PRAHA a.s. and the Karlsruhe Institute of Technology.

CLADDING BEHAVIOUR UNDER LOCA ACCIDENT

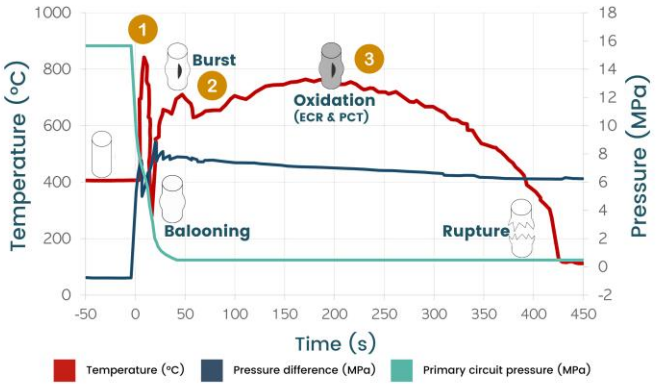

1 **Differential thermal analysis** (DTA) was performed to determine the melting point of the alloy. The sample of Cr-Ni alloy and the reference alumina powder were weighted and placed symmetrically in the STA 449 F3 Jupiter Eco from the NETZCH company facility. The furnace was programmed to heat up to 1450°C (30 K/min) and cool down to 100°C (100 K/min). During the process, a differential thermocouple was set to detect the temperature difference between the sample and the reference powder.

2 During the first peak of the LOCA accident, the fuel cladding under high inner pressure and increasing temperature undergoes ballooning and eventually, it may burst. The so-called **burst test** simulates this phenomenon. The reference and the Cr-Ni specimens were sealed to the argon-containing reservoir at the required gas pressure. Each specimen was equipped with K-thermocouple. Afterwards, the specimen was inserted into the pre-heated resistance furnace with a predefined temperature zone. Temperature and inner gas pressure propagation were measured online. The experiments were done at several temperature levels between 900 and 1050 °C with internal pressure from 1 to 10 MPa, in an argon environment. The experiments were terminated after cladding failure and consequent pressure decrease.

3 **The oxidation kinetics** were determined using continuous gravimetric measurements. The experimental facility consisted of a thermal balance STA 449 F3 Jupiter from NETZSCH company, the steam generator from Bronkhorst Company, and a quadrupole mass spectrometer NETZSCH QMS 403 C. A set of isothermal experiments at 700, 800, 900, 1000, 1100 and 1200 °C was performed. After that, the obtained data were analysed, and the expected corrosion rate was calculated based on the specific oxidation behaviour by means of parabolic or linear kinetics [2].

[1] Chalupová A., Steinbrück M., Grosse M., Krejčí J., Ševeček M. High-Temperature Oxidation of Chrome-nickel alloy. Acta Polytechnica CTU Proceedings. 2020, 28. ISSN 2336-5382.

[2] B. Pieraggi, „Calculations of Parabolic Reaction Rate Constants," v Oxidation of Metals, sv. 27, 1987.

MATERIAL

Segments of the alloy were cut from non-irradiated longer tubes, deburred, ground, and cleaned in acetone. The geometry of the tested specimens was cylindrical, with an outer diameter of 8.3 mm, and an inner diameter of 7.1 mm.

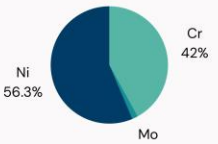

The chemical composition of the Cr-Ni alloy used for experiments

RESULTS

Generally, melting causes an endothermic reaction (peak upwards). Therefore it was determined as 1356.7 °C. On the other hand, solidification causes an exothermic reaction (downward peak). Thus, according to the graph, it started at a lower temperature of 1355.8 °C. In comparison, the melting point of zirconium alloy reaches 1850 °C. However, since the exothermic oxidation rate of Ni-Cr alloy is far more moderate than in the case of zirconium cladding, the melting temperature is expected to be reached later in a typical accident scenario. Consequently, the lower melting point may not be a limiting factor for ATF requirements.

The oxidation kinetics of the Cr-Ni alloy was studied in the temperature range from 700 °C to 1200 °C. The alloy exhibited rather linear kinetics after oxidation in steam at temperatures 700 °C and 800 °C.

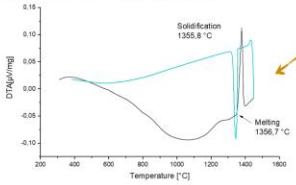

At temperatures from 900 °C to 1200 °C, the oxidation rate of the alloy starts to be controlled by diffusion, and thus it resembles parabolic kinetics. It was confirmed that the Cr-Ni has meagre weight gain under high-temperature oxidation. The figure beneath shows the Arrhenius plot for various proposed ATF designs (Cr-Ni. FeCrAl, Inconel 617) compared to standard Zr-based cladding materials (Zr1%Nb, Zircaloy-4) and Cathcart-Pawel correlation. On the whole, all potential ATF materials outperform Zr-based alloys. The Arrhenius equation has been used to determine the activation energy from experiments at isothermal temperatures.

The burst test has shown the extreme resistance of Cr-Ni alloy compared to zirconium alloy. The results of time to burst and uniform deformation after the experiment were used to determine the creep rate of the cladding.

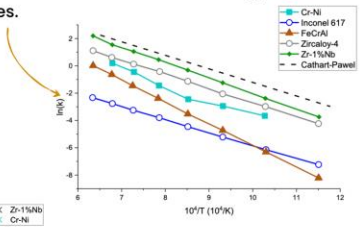

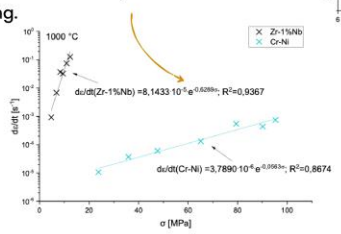

CONCLUSION

Obtained results show a better resistance of Cr-Ni alloy compared to zirconium alloys during high-temperature oxidation in steam and creep tests. All visual evaluation, deformation, microstructure analysis, and weight gain, together with the derived oxidation kinetics parameters confirmed its stability under severe accident conditions. These conclusions confirm that Cr-Ni is a promising ATF material candidate.

The main disadvantage of the alloy is the high cross-section of thermal neutrons. Accordingly, a few possible ideas on how to improve the alloy's neutron performance were introduced. It has been decleared that the alloy allows a thinner wall of the cladding compared to zirconium. However, sufficient compensation for the high thermal neutron absorption requires a substantial increase in fuel enrichment. The alloy is often associated with fourth-generation reactors. An implementation of high-density fuel instead of uranium dioxide pellets increases the capacity of uranium. Hence the usage of the oxidation-resistant Cr-Ni alloy as a cladding material could be a possible way to achieve a highly efficient and essentially safe fuel system.

USE OF NATURAL CIRCULATION IN SAFETY SYSTEMS OF SMALL MODULAR REACTORS

Yehor CHEPLAKOV

Department of Nuclear Power Plants, National University of Odessa Polytechnic, Odessa, Ukraine

Use of natural circulation in safety systems of small modular reactors. The article substantiates the reason for the use of natural circulation in the safety systems of nuclear power plants to divert residual energy after the cessation of the nuclear fission chain reaction. A brief description of the principle of natural circulation, a description of the process, the causes, the conditions of its support. An analysis of the conditions of natural circulation in one of the safety systems of a small modular reactor developed by the American company NuScale is also presented.

USE OF NATURAL CIRCULATION IN SAFETY SYSTEMS OF SMALL MODULAR REACTORS

INTRODUCTION

Use of natural circulation in safety systems of small modular reactors. The article substantiates the reason for the use of natural circulation in the safety systems of nuclear power plants to divert residual energy after the cessation of the nuclear fission chain reaction. A brief description of the principle of natural circulation, a description of the process, the causes, the conditions of its support. An analysis of the conditions of natural circulation in one of the safety systems of a small modular reactor developed by the American company NuScale is also presented.

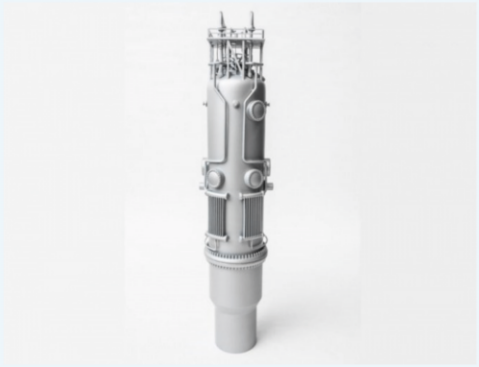

The NuScale Small Modular Reactor has two main passive safety systems:
- Emergency Core Cooling System;
- Residual Heat Removal System.

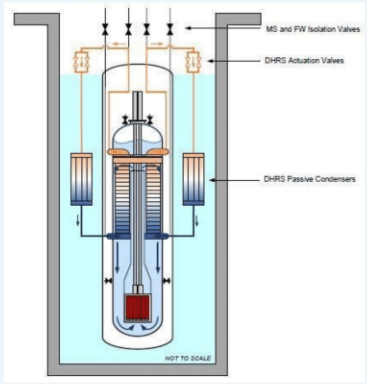

Both use the principle of natural circulation.
My master's work is devoted to the second system. The system was analyzed in the work: its components, the principle of operation. Data were also collected for the calculation (most of the data is not available for public use, so they were accepted by me based on five years of training experience, so the work is inventive in nature.
The second figure shows a diagram of the reactor as well as the DHRS.

CALCULATED PART

Two calculations were made. The condition of the first - the coolant is a single-phase medium, the second - two-phase.

In both calculations, the condition of natural circulation is equality:

$$P_{dv} = \Sigma P, \quad (1)$$

where P_{dv} - driving pressure of natural circulation, kPa;

ΣP- total hydraulic resistance of the natural circulation circuit, kPa.

In the case of equality, a constant process of natural circulation of the DHRS system is ensured.

In the calculations, it was assumed that the heat of the residual energy of the core is completely removed through the steam generator. Thus, the calculation was simplified to the calculation of the circuit, including the steam generator and TOAR.

The calculation process took into account:

- thermal capacity of the reactor;
- coefficient of local resistance of all elements;
-temperature at the inlet / outlet of the steam generator (if you accept the condition described above, the temperature can be taken equal to the inlet / outlet of the core);
- temperature at the inlet / outlet of the TOAR;
- number of turns and bends of the pipeline;
- pressure in the circuit;
- cross-sectional area of the steam generator; cross-sectional area of TOAR;
- height difference between hot and cold springs;
- height (length) of the cold source;
- height (length) of the hot spring;
- diameter of connecting pipes;
- length of connecting pipes;
- pressure in the pool;
- temperature in the pool.

The technique includes the thermal and hydraulic design parts of the steam generator and passive condenser. The result is a graph of two functions.

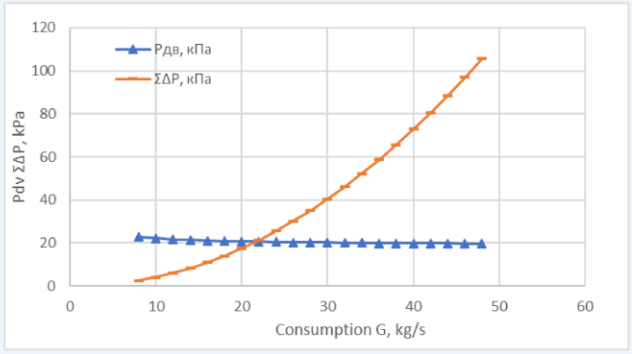

Graph of the dependence of the driving pressure on the flow rate and the total hydraulic resistance on the flow rate in single-phase (water) movement of the coolant

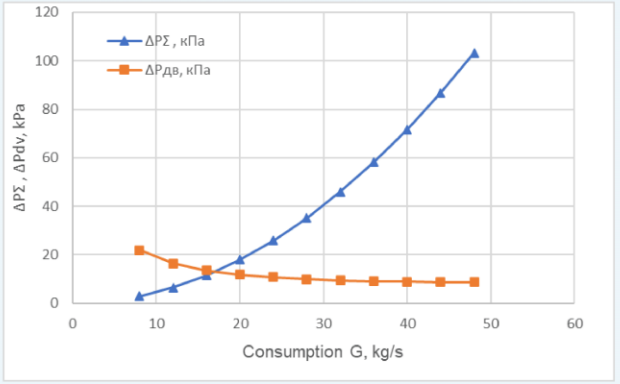

Graph of the dependence of the driving pressure on the flow rate and the total hydraulic resistance on the flow rate in two-phase movement of the coolant

CONCLUSION

In the single-phase flow of the coolant (water), the curves intersect at a flow rate of 22 kg / s. It is at this value that equality (1) holds. The graphs show that the value of the driving pressure (RDV) decreases with increasing flow rate, this is due to the fact that the density of the coolant decreases over time, as a consequence of increasing the temperature value with increasing flow rate. The increase in temperature is due to a decrease in the amount of heat dissipation due to the gradual increase in the speed of the coolant. The values of the total hydraulic resistance of the NC circuit ($\Sigma\Delta P$) increase as the flow rate increases, as the speed increases and as a result the friction forces of the surfaces of pipelines and heat exchangers increase (increasing their hydraulic resistance).

In the two-phase flow of the coolant (water), the curves intersect at a flow rate of 18 kg / s, while equality (1) is satisfied.

The basis of natural circulation is the general physical law of universal gravitation, from which it follows that the greater the mass of the object, the stronger the gravitational force acts on it. Changing the level of residual energy directly affects the temperature at the entrance to the hot source (steam generator) MMP, thereby changing the intensity of the process.

After calculating and evaluating the results, we can conclude that the single-phase medium (water) has a better effect on the process of natural circulation due to better heat dissipation from the heat transfer surface. This is directly affected by the density of the medium, as well as homogeneity, because the heat dissipation of steam will be much worse than water.

From the conducted research, in particular, it follows that the competent arrangement of the equipment and the difference of heights provides a stable NC process without the use of pumps and additional energy for pumping the coolant. NC - the future of safety systems for nuclear reactors, the impact of the human factor in it is minimized, which is one of the fundamental principles of safety of nuclear power plants.

CONTACTS

Cheplakov Yehor Student - Master of the Department of Nuclear Power Plants, National University of Odessa Polytechnic, Ukraine. Email: cheplakov1999@gmail.com

The diploma project was developed under the guidance of Yury Komarov - Doctor of Technical Sciences, Associate Professor of the Department of Nuclear Power Plants, National University Odessa Polytechnic, Ukraine. Email: komarov@op.edu.ua

Head of the graduation project Korolev Alexander - Professor of the Department of Nuclear Power Plants, National University of Odessa Polytechnic, Ukraine. Email: korolyov118@gmail.com

THE EFFECT OF HYDROGEN CONTENT ON FUEL CLADDING MATERIALS PROPERTIES USED IN PRESSURISED WATER COOLED NUCLEAR REACTORS

Alžběta ENDRYCHOVÁ

Department of Energy Engineering, Faculty of Mechanical Engineering,
Czech Technical University in Prague, Prague, Czech Republic

Fuel cladding serves as the first protective barrier against the release of fission products into the environment outside the nuclear power plant. Zirconium-based alloys are preferred because of their lower thermal neutron absorption cross section, relatively high melting temperature, and good corrosion and fracture resistance.

These zirconium alloys degrade during reactor operation due to irradiation, corrosion or mechanical damage. One of the factors that affect the integrity of the fuel cladding is hydrogen absorption, during which hydrogen exceeds its terminal solid solubility of precipitation. Depending on the concentration and temperature, the hydrogen creates localized zirconium hydrides that embrittle the cladding and can cause its failure.

The effect of hydrogen content on fuel cladding materials properties used in pressurised water cooled nuclear reactors

Alžběta Endrychová, Master's Thesis, 2022

Department of Energy Engineering, Faculty of Mechanical Engineering, CTU in Prague

CTU CZECH TECHNICAL UNIVERSITY IN PRAGUE

Objectives

1. Review of the most commonly used zirconium alloys for fuel cladding and the requirements for material used for fuel cladding.
2. Study of mechanical properties and microstructural changes of zirconium alloy for the following temperatures: 350, 450 and 550 °C.
3. Observation of the behaviour and growth of the oxide layer depending on the hydrogen content.

Introduction

Fuel cladding serves as the first protective barrier against the release of fission products into the environment outside the nuclear power plant. Zirconium-based alloys are preferred because of their lower thermal neutron absorption cross section, relatively high melting temperature, and good corrosion and fracture resistance.

These zirconium alloys degrade during reactor operation due to irradiation, corrosion or mechanical damage. One of the factors that affect the integrity of the fuel cladding is hydrogen absorption, during which hydrogen exceeds its terminal solid solubility of precipitation. Depending on the concentration and temperature, the hydrogen creates localized zirconium hydrides that embrittle the cladding and can cause its failure.

Material

For the experimental part was chosen Zr1Nb alloy which is used in Czech nuclear power plants. This alloy contains 1 wt.% of niobium which improves its mechanical and corrosion properties. It also prevents spalling of the oxide layer and reduces the amount of hydrogen diffusing into the alloy during irradiation in the reactor.

Experimental methods

The following methods were chosen to study the microstructure and mechanical properties of Zr1Nb alloy:

- Annealing (350, 450, 550°C),
- Microhardeness tests (Vickers),
- Scanning Electron Microscophy (SEM),
- Tensile tests.

Samples

For the preparation of the samples were used tubes with a diameter of 9.1 mm and a thickness of 0.57 mm:

- without hydrogen content,
- deformed by four-point flexural test with hydrogen content of 0, 400 and 610 ppm (see Figure 1, 2),
- with hydrogen content from 0 to 652 ppm (see Figure 3).

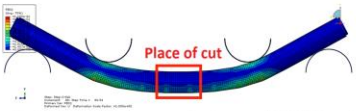

Figure 1: Deformed tube by four-point flexular test (ABAQUS simulation).

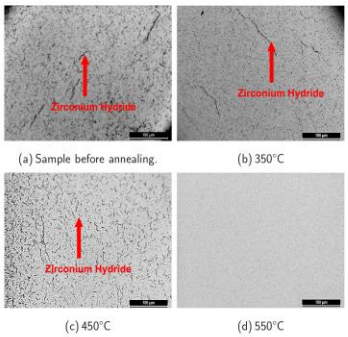

(a) Sample before annealing. (b) 350°C (c) 450°C (d) 550°C

Figure 2: Sample Zr1Nb with hydrogen content of 400 ppm (LOM images) before and after annealing.

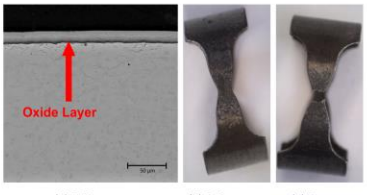

(a) SEM image (b) Deformation (c) Fracture

Figure 3: Sample after tensile test with hydrogen content of 411 ppm.

Microhardeness and Microstructure

In Figures 4 a local increase of microhardness can be seen at the location of maximal plastic deformation for the speciment with hydrogen content of 400 ppm after four-point flexure test. In addiction, the effect of annealing temperature above 550°C reduced the number of dislocations and causes a uniform distribution of hydrides which can be seen in Figure 5. In Figures 2 and 5 are SEM images from which it can be seen that the annealing temperatures did not change microstructure of the sample.

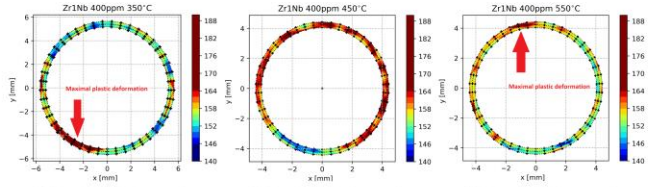

(a) Sample annealed at 350 °C. (b) Sample annealed at 450 °C. (c) Sample annealed at 550 °C.

Figure 4: Microhardness distribution maps and of Zr1Nb samples with a hydrogen content of 400 ppm after annealing.

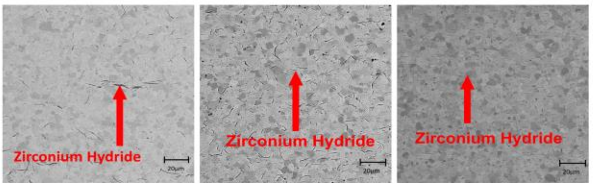

(a) Sample annealed at 350 °C. (b) Sample annealed at 450 °C. (c) Sample annealed at 550 °C.

Figure 5: SEM images of Zr1Nb samples with a hydrogen content of 400 ppm after annealing.

Oxide layer

From the dependence of the thickness of the oxide layer on the hydrogen content, which is shown in Figure 6, it is apparent that the thickness increases with increasing hydrogen content.

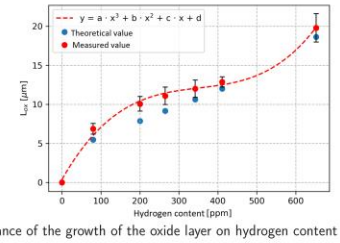

Figure 6: Dependance of the growth of the oxide layer on hydrogen content from 0 to 652 ppm.

Tensile tests

As the hydrogen content increases, both the yield strength and the ultimate tensile strength decrease (see Figure 7). Thus, the effect of hydrogen embrittlement becomes apparent. In the contrary, the sample with 652 ppm hydrogen content showed a different behaviour, where both yield and ultimate tensile strength increased due to the higher hydrogen content and the higher thickness of the oxide layer. All of this has the effect of strengthening the wall of the sample, but at the same time the sample becomes more brittle.

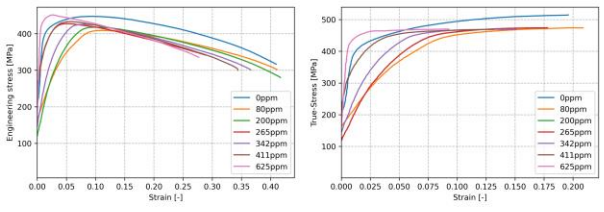

(a) Stress-Strain curve. (b) True Stress-Strain curve.

Figure 7: Results from tensile tests for samples with hydrogen content from 0 to 652 ppm.

Conclusion

- Annealing temperatures of 350, 450 and 550°C don't change microstructure of Zr1Nb alloy.
- The zirconium hydrides are gradually dissolved by annealing and distributed evenly.
- The effect of annealing temperature above 550°C reduces the number of dislocations and results in a reduction of stress around the perimeter of the sample.
- The thickness of the oxide layer increases with increasing hydrogen content.
- The yield strength and ultimate tensile strength decreases with increasing hydrogen content.

DESIGNING A TOP COOLING SYSTEM FOR AN ELECTROMAGNETIC CALORIMETER

Matěj JEŘÁBEK

Faculty of Mechanical Engineering, University of West Bohemia, Pilsen, Czech Republic

In order to collect all the necessary information from antiproton-proton collisions, an EMC (Electro Magnetic Calorimeter) will be built as a part of the PANDA detector. The EMC will be able to provide accurate trajectory reconstruction, energy and momentum measurements and very efficient identification of the charged particles. The electromagnetic calorimeter works on the principle of scintillation, i.e., the radiation emitted by the particle collisions reacts with a scintillator that produces a series of flashes of different intensities. These flashes are captured by electronics and transformed into a digital signal. The EMC uses hundreds of cube-shaped scintillators made of $PbWO_4$, whose scintillation properties are strongly dependent on temperature. This poster briefly shows the design of a cooling system that would allow low crystal temperatures to be maintained, and homogeneous distribution and stability of the temperature over all the crystals while the detector is in operation. Furthermore, this poster shows the analysis of the effect of the pressure drop of the whole cooling system, from which the design and requirements for the main pump of the system are then derived.

DESIGNING A TOP COOLING SYSTEM FOR AN ELECTROMAGNETIC CALORIMETER

MATĚJ JEŘÁBEK

JADERNÉ DNY
FAKULTA STROJNÍ ZÁPADOČESKÉ UNIVERZITY V PLZNI

INTRODUCTION

In order to collect all the necessary information from antiproton-proton collisions, an EMC (Electro Magnetic Calorimeter) will be built as a part of the PANDA detector. The EMC will be able to provide accurate trajectory reconstruction, energy and momentum measurements and very efficient identification of the charged particles. The electromagnetic calorimeter works on the principle of scintillation, i.e., the radiation emitted by the particle collisions reacts with a scintillator that produces a series of flashes of different intensities [2]. These flashes are captured by electronics and transformed into a digital signal. The EMC uses hundreds of cube-shaped scintillators made of PbWO4, whose scintillation properties are strongly dependent on temperature. This poster briefly shows the design of a cooling system that would allow low crystal temperatures to be maintained, and homogeneous distribution and stability of the temperature over all the crystals while the detector is in operation. Furthermore, this poster shows the analysis of the effect of the pressure drop of the whole cooling system, from which the design and requirements for the main pump of the system are then derived.

DESCRIPTION OF THE PANDA DETECTOR

HESR is one of the accelerators located in the newly built FAIR complex. Its main components are the PANDA detector and the Koala detector which is used to measure the differential cross section of antiproton-proton elastic scattering [1]. The PANDA detector is composed of several large systems. However, in this poster we will focus only on the calorimeter of which the proposed cooling system will be a part. Calorimeter can be seen in FIGURE 2 [3].

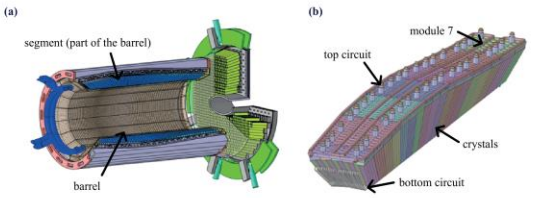

FIGURE 2. Left (a): Electromagnetic calorimeter model [3]. Right (b): Segment detail

COOLING SYSTEM OVERVIEW

The primary task of the cooling system is to maintain a very low, stable temperature and homogeneous temperature distribution over all the crystals. The cooling capacity requirements of the system are determined by the heat sources present in the calorimeter segments. These sources are the measuring or sensing electronics chips, which can be seen in FIGURE 3a, and the bus cables. As an additional source of heat, it is necessary to consider the heat that enters the measuring compartment via conduction from the surroundings. The second main task is to design the cooling systems depending on the total pressure drop, which will ultimately influence the selection of the main pump of the system. The cooling system is schematically shown in FIGURE 3b.

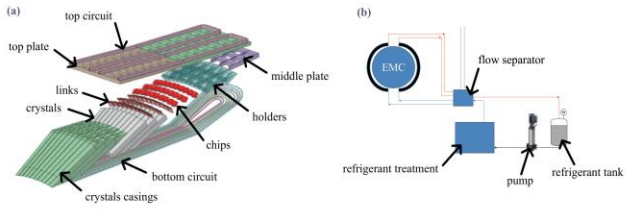

FIGURE 3. Left (a): Parts of the module 7. Right (b): Cooling system schematics [4]

COOLING SYSTEM REQUIREMENTS

TABLE 1 Summary of requirements [4]

t [°C]	Δt [°C]	Δp [bar]	$\dot{m}$ [kg/s]
-30 to -20	≤1	≤1	≤2.78

COOLING SYSTEM WORKING MEDIUM

TABLE 2 Material properties of the refrigerant [4]

Medium	c_p [J/(kg·K)]	ρ [kg/m³]	μ [Pa·s]	λ [W/m·K]	M [kg/mol]
water/methanol (40/60)	3151	930	$7.7e^{-3}$	0.341	26.5

TEMPERATURE FIELD ANALYSIS

From FIGURE 5 it can be seen that the temperature difference between all the crystals is now 0.3 °C, and so it can be concluded that the requirement for a maximum temperature difference across all the crystals of up to 1 °C is satisfied.

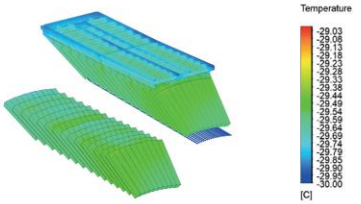

FIGURE 5. Temperature field distribution

PRESSURE LOSS ANALYSIS

The results from the stationary CFD simulations of the flow field show that the customer's requirements for the total pressure drop of the cooling system were not met. In the context of these results, it can be further stated that the customer's required pressure drop of the entire cooling system is an initial conceptual requirement. This consideration is also related to the finding that even the pressure drop of a single tube of the upper cooling circuit alone is not able to meet the requirements for a total pressure drop value of $\Delta p \leq 1$ bar.

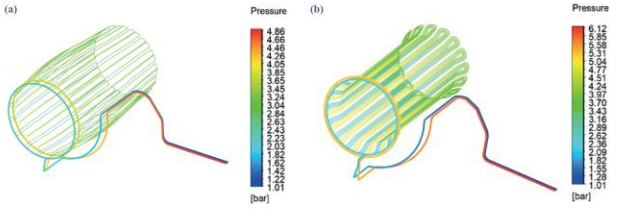

FIGURE 9. Left (a): Pressure field of upper cooling system. Right (b): Pressure field of bottom cooling system

CONCLUSION

The main task of the work was to design a cooling system that could keep scintillator crystals at a temperature between -30 °C and -20 °C during the operation of the calorimeter, so that the difference between the maximum and minimum temperature of all the crystals does not exceed 1 °C. From this point of view, this work was successful, as by adding a bottom cooling system to the initial computational domain, this condition was met, and the maximum temperature difference across all the crystals is now 0.3 °C. In terms of pressure drop, the customer's requirements have not yet been met, but the requirement that the total pressure drop in the cooling system should not exceed 1 bar appears to be unrealistic, as even the pressure drop of a single tube in the system is approximately 1.13 bar. In view of this fact, the initial requirements have to be reconsidered and modified to take into account the priorities in the system design, which is temperature stability.

REFERENCES

1. BELIAS, Tassos a PETERS, Klaus.. PANDA Annual Report. [Online] 2021. [Citace: 5. 1. 2021.] Available from: https://panda.gsi.de/system/files/user_uploads/k.peters/RE-MGM-2020-002.pdf.

2. VOLF, Michal. AIP Conference Proceedings. CFD Simulation of The Cooling System of a Calorimeter Detector. [Online] 2021. [Citated: 25. 3. 2021.] Available from: https://doi.org/10.1063/5.0041387.

3. —. Chlazení Elktromagnetického Kalorimetru PANDA s Českou Stopou. Plzeň : ZČU, 2019.2021.] Available from: https://doi.org/10.1063/5.0041387.

4. ROSIER, P. FOSWIKI. Definition of The Chiller of The Cooling Plant. [Online] 2014. [Citace: 27. 3. 2021.] Available from: https://panda-wiki.gsi.de/foswiki/pub/EMC/Cooling/EMC-COOLING-Plant-Chiller-140113.pdf.

PRINTED CIRCUIT HEAT EXCHANGER (PCHE) DESIGN CODE DEVELOPMENT IN PYTHON LANGUAGE

Matyáš JUNEK

Department of Energy Engineering, Faculty of Mechanical Engineering,
Czech Technical University in Prague, Prague, Czech Republic

Printed circuit heat exchangers belong to the group of compact heat exchangers (HE) (high ratio of heat transfer area and volume of HE). PCHE consists of thick plates with chemically etched microchannels, in which fluid flow. Plates for hot and cold fluid are stacked to each other and then diffusion bonded. Diffusion bonding is a special welding process with operational temperatures below the melting point and it's causing strain growth over borders of adjacent plates. This technique results in high integrity, high strength HE ideal for high pressure and high-temperature applications. That is the reason why PCHEs are considered for indirect Brayton cycles with supercritical carbon dioxide (sCO_2). It would be beneficial to be able to determine the size of PCHE for given parameters. For that purpose Python code was written.

Printed circuit heat exchanger (PCHE) design code development in Python language

Matyáš Junek, Master's Thesis, 2022

Department of Energy Engineering, Faculty of Mechanical Engineering, CTU in Prague

CTU
CZECH TECHNICAL UNIVERSITY IN PRAGUE

Objectives

1. Review of thermohydraulic performance of PCHE with gasses as working fluids.
2. Develop a program for computing the size of PCHE for given boundary conditions.
3. Thanks to the written code determine dimensions of He/sCO_2 PCHE in future fusion power plant DEMO.

Introduction

Printed circuit heat exchangers belong to the group of compact heat exchangers (HE) (high ratio of heat transfer area and volume of HE). PCHE consists of thick plates with chemically etched microchannels, in which fluid flow. Plates for hot and cold fluid are stacked to each other and then diffusion bonded. Diffusion bonding is a special welding process with operational temperatures below the melting point and it's causing strain growth over borders of adjacent plates. This technique results in high integrity, high strength HE ideal for high pressure and high-temperature applications. That is the reason why PCHEs are considered for indirect Brayton cycles with supercritical carbon dioxide (sCO2). It would be beneficial to be able to determine the size of PCHE for given parameters. For that purpose Python code was written.

Printed circuit heat exchanger

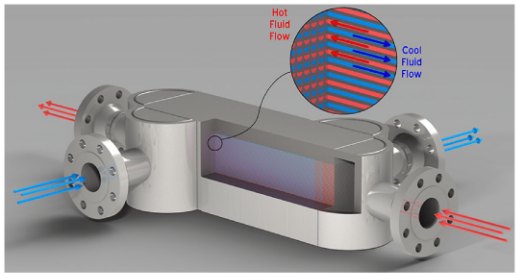

Figure 1: Printed circuit heat exchanger

Program concept

The program for computing the size of PCHE is written in the Python program language. The program starts by entering input parameters, for example, inlet and outlet temperatures, pressures, the effectiveness of PCHE, or maximum allowable pressure drop. The first step is to compute basic heat balance. After that, optionally mechanical design can be computed. The next step is to estimate the heat transfer area and free flow area. Estimation significantly decreases computational time. Then the main part of the program follows. Overall enthalpy is divided into *n* nodes (fig 2). In each node fluid properties, thermohydraulic characteristics, and length of the node are determined. When whole HE is computed, given pressure drop and maximum allowable pressure drop are compared. If they are approximately equal results and data are written to a file. Otherwise, certain parameters are changed and the next iteration starts. Fluids' properties are determined due to the CoolProp library. Several geometries of channels can be computed: Straight or "zigzag" with wave angle 32.5°or 40°. For each geometry proper correlation was used [1][2].

Computational schema

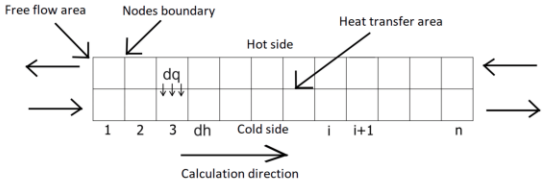

Figure 2: Computational schema

Validation and program usage

The program was validated due to experiments with PCHE in He/He loop. There was 16 experiments total. Measured experimental data such are inlet and outlet temperatures, pressure drop or thermal power was used as inputs for the program. Computed size of PCHE was compared with size of actual experimental PCHE. Results shows that maximum deviation of computed and actual volume of compared PCHEs is 2.4%. Thus the program can be considered validated. The software was then used to determine size of heater in Brayton sCO_2 secondary circuit for future fusion power plant DEMO. Input parameters were provided by Štěpánek [3].

Dependence of effectiveness and volume

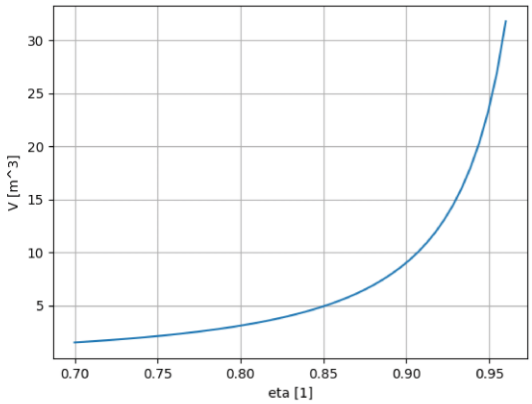

Figure 3: Dependence of effectiveness and volume

Conclusions and discussion

- The program for computing the size of different PCHE geometries for given parameters was developed and validated. It can be used and enhanced for future projects.
- Results of computing shows that if PCHE were used for a secondary circuit with sCO2 as a working fluid in the future fusion power plant DEMO 40 He/sCO2 parallel heaters with dimensions 6.61 x 0.6 x 1.32 m would be needed. These heat exchangers would have zigzag geometry of microchannels with a wave angle 40°and a double plate for the hot side.
- Presented results are valid for given input parameters. Actual dimensions in DEMO could be different if demanded properties will be different. For example, the Overall volume of HE strongly depends on the required effectiveness of PCHE as shown in fig 3.

References

[1] Lei Chai and Savvas A. Tassou.
A review of printed circuit heat exchangers for helium and supercritical co2 brayton cycles.
Thermal Science and Engineering Progress, 18:100543, 2020.

[2] Seong Gu Kim, Youho Lee, Yoonhan Ahn, and Jeong Ik Lee.
Cfd aided approach to design printed circuit heat exchangers for supercritical co2 brayton cycle application.
Annals of Nuclear Energy, 92:175–185, 2016.

[3] Jan Stepanek, Slavomir Entler, Jan Syblik, Ladislav Vesely, Vaclav Dostal, and Pavel Zacha.
Comprehensive comparison of various working media and corresponding power cycle layouts for the helium-cooled demo reactor.
Fusion Engineering and Design, 166:112287, 2021.

matyas.junek@fs.cvut.cz

SIMULATION OF MELT FORMATION AND PROPAGATION IN SEVERE ACCIDENTS OF NUCLEAR REACTORS

Jan KOMRSKA

Department of Energy Engineering, Faculty of Mechanical Engineering,
Czech Technical University in Prague, Prague, Czech Republic

ALLEGRO is gas cooled fact reactor (GFR) demonstrator currently developed by the V4G4 Centre for Excellence group. Its main purpose is to demonstrate technologies and materials for GFR, to gain knowledge and operational experience with this type of reactor. Same as any new type of reactor it is equipped with many advanced safety systems, including a system for localization and stabilization of corium melt - core catcher.

Simulation of melt formation and propagation in severe accidents of nuclear reactors

Jan Komrska, Master's Thesis, 2022

Department of Energy Engineering, Faculty of Mechanical Engineering, CTU in Prague

CTU
CZECH TECHNICAL UNIVERSITY IN PRAGUE

Abstract

The Master's Thesis is focused on description of severe accident scenario with melting and propagation of corium melt in core catcher of reactor ALLEGRO. We utilize two consecutive numerical calculations. The first part of the calculation is solved using MELCOR 2.2 code. The consequential part is solved in CFD program ANSYS Fluent.

Introduction

ALLEGRO is gas cooled fact reactor (GFR) demonstrator currently developed by the V4G4 Centre for Excellence group. Its main purpose is to demonstrate technologies and materials for GFR, to gain knowledge and operational experience with this type of reactor. Same as any new type of reactor it is equipped with many advanced safety systems, including a system for localization and stabilization of corium melt - core catcher.

ALLEGRO Core Catcher Geometry

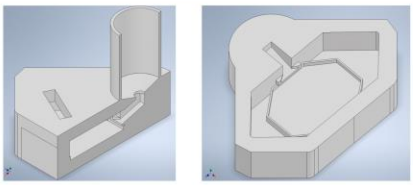

Figure 1: ALLEGRO Core Catcher Geometry

Core catcher is a safety system designed to catch and cool corium during a severe accident with core meltdown. For the purposes of simulation of corium behavior in core catcher structure there was a need to make two different models in two different codes. The first model deals with corium creation and its interaction with sacrificial materials on the bottom of reactor shaft. Second model was used to describe corium flow in core catcher structure.

MELCOR Nodalization and Solution

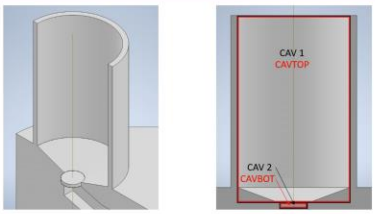

Figure 2: MELCOR Nodalization scheme

MELCOR simulation consists of corium interaction with sacrificial materials located on the bottom of reactor shaft and melt plug. The purpose of the melt plug is to hold the corium melt for time needed to accumulate most of the corium from the reactor pressure vessel. It was calculated that this process of corium accumulation should take 1010 seconds and this information was used to define the simulation time. The main purpose of this simulation is to find properties of corium. These properties are then used in the consequential CFD simulation.

MELCOR Results

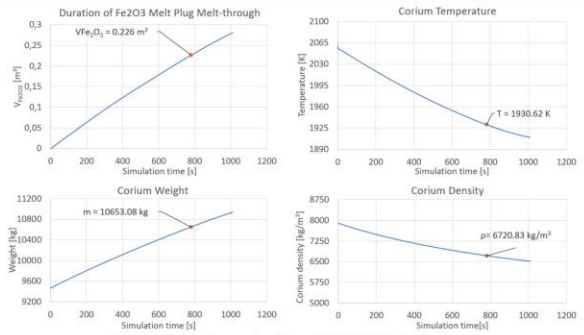

Figure 3: Main results from MELCOR simulation

During the simulation it was found that the melt plug is inadequate because the corium melted through the melt plug in 760 seconds. Corium properties have been calculated as following:

Corium Temperature :	1930.62 K
Corium Density :	6720.83 kg.m^{-3}
Corium Weight :	10653.08 kg
Weight of molten Fe_2O_3 :	1230.08 kg
Volume of Corium :	1.585 m^3

CFD Geometry and Solution

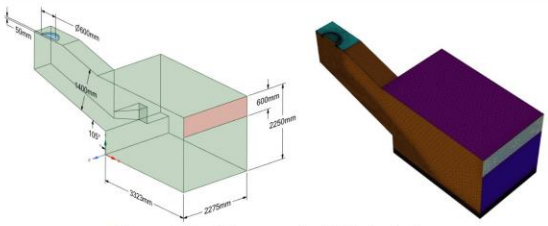

Figure 4: Used Geometry for CFD simulation

This simulation consists of corium flow through melt discharge channel and into the core catcher spreading compartment. Simulation describes two phase flow of corium and nitrogen atmosphere. Due to high complexity of simulating two phase flow and complex properties of corium there were used a few simplifying conditions. Since main purpose of the simulation was to describe very dynamic process of corium flow during first moments after melt plug failure we were able to use smaller portion of total volume of the core catcher geometry. Using this simplified geometry we were able to drastically reduce total computational time and thus enhance CFD capabilities for this simulation. Second simplifying condition was used to simplify properties of corium, including melt stratification and creation of crust at the edges of corium - these properties can't be directly simulated using CFD.

CFD Results

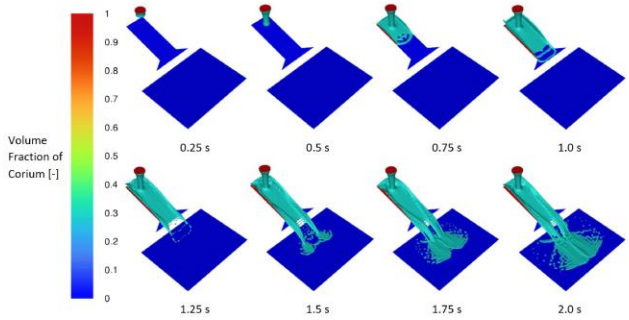

Figure 5: Sequence of Corium flow through Core Catcher Structure

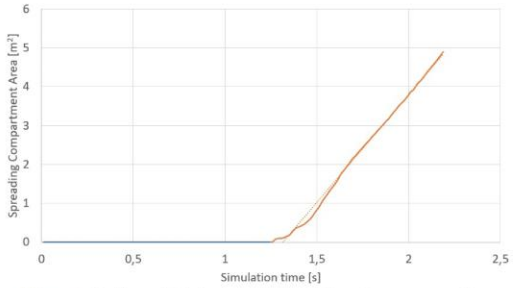

Figure 6: Spillage of Corium on the Spreading Compartment floor

Results of CFD simulation are presented as a graphical sequence of corium flow and graph of spreading compartment area that is occupied by corium melt. Simulation time is set by condition of corium flow reaching edges of computational mesh. Corium reaches mesh edges at 2.18 seconds. At 2.18 seconds the corium will spread on 4.843 m^2. Following this corium spreading trend we can simply aproximate that the core catcher spreading compartment of 54.2 m^2 will be filled at 12.33 seconds.

Conclusion

This thesis is focused on simulation of complex corium behavior including corium melt formation and propagation during severe accident with core meltdown. Due to complexity of observed phenomena the simulation had to be divided into two separate models using two different codes. The results of this thesis can be used for design improvements of ALLEGRO core catcher. Further, this work will be expanded upon by including used simplifications into a more complex simulation of corium behavior in ALLEGRO Core Catcher.

References

1. ZÁCHA, Pavel, Václav ŽELEZNÝ, a GUK CHOL JUN. CFD model rozlivu koria v šachtě reaktoru JE Temelín. Research report. 12115-JE/2019/01. Praha: ČVUT v Praze. 2019.
2. HUMPRIES, L.L. MELCOR Computer Code Manuals Vol. 1: Primer and Users' Guide. B.m.: Sandia National Laboratories. 2017
3. Ansys Fluent Theory Guide, Release 2021 R2 . Ansys Inc., Southpointe, 2600 Canonsburg, PA 15317, USA, July 2021.
4. CAD model of ALLEGRO Core Catcher, ÚJV Řež a.s., 2021

jan.komrska@fs.cvut.cz

INCREASE OF THE STEAM GENERATORS PGV – 1000 RESOURCE

Yevhen KUZOMA

Zaporizhzhia Nuclear Power Plant, Energodar, Zaporozhye region, Ukraine
West Bohemian University, Faculty of Mechanical Engineering, Pilsen, Czech Republic

The presented paper focuses on the flow of the coolant behind a grid containing mixing elements. Examination of the flow field was performed using the experimental method stereo PIV. The goal of the study was to evaluate the influence of the geometry and the position of individual turbulizers (blades) on the current field behind the grids. The measurement was performed on an experimental track. Design of the grids is based on fuel assemblies intended for a nuclear reactor of the VVER 1000 type. Results obtained from the measurement of two types of grids at several distances correspond to the course given by the grid manufacturer. Results of the experiments were compared with CFD simulations.

NUCLEAR DAYS 2022
UNIVERSITY OF WEST BOHEMIA IN PILSEN, CZECH REPUBLIC

Increase of the steam generators PGV-1000 resource

Kuzoma Yevhen
Zaporizhzhia Nuclear Power Plant, Energodar, Zaporozhye region, Ukraine
Doctoral student West Bohemian University, Faculty of Mechanical Engineering, Pilsen, Czech Republic
kuzomazhenya@gmail.com

Introduction

According to the task, a technical solution was developed to increase the service life of PGV-1000.

Steam generators are an integral part of the primary and secondary circuits, they are a physical barrier between the radioactive and non-radioactive parts of nuclear power plants operating under difficult conditions in terms of temperature, dynamic, hydraulic, corrosion processes and the impact on metal. The steam generator PGV-1000M is designed to generate saturated steam as part of a NPP power unit with a water-cooled power reactor VVER and is an integral part of the main circulation circuit.

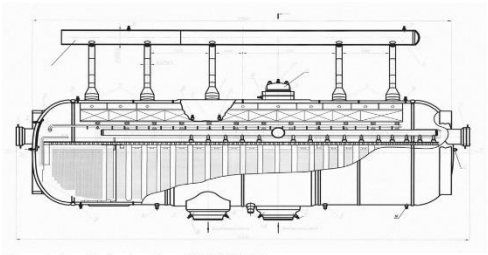

Figure 1. Longitudinal section of PGV-1000M

Initial state of the SG purge system

Operating experience has shown that part of the SG failed and was replaced without having worked out the specified resource due to leaks in the collectors and the pipe system. Therefore, special attention is paid to the reliability of SGs.

During the operation of steam generators during corrosion surveys and inspections using television, it was noted the presence of a large amount of sludge on the bottoms of the steam generators and in the annulus. The reason for this was that the removal of salts and sludge from the steam generator was not effective.

To increase the efficiency of sludge removal and removal of salts with purge water, it is necessary to separate the purge lines from the "pockets" of the SG headers and ends, with the installation of electric actuators outside the steam generator box.

At the time of the design and construction of the ZNPP power units, the steam generator blowdown consisted of one line, into which two blowdown lines were assemb from the sides of the SG and one line from the "pockets" of the "cold" and "hot" collect as well as the steam generator drainage line with cut-off valves.

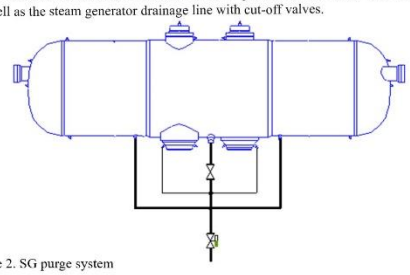

Figure 2. SG purge system

Organization of continuous and periodic purge

Then, according to the "Measures to improve the reliability and ensure the operational life of steam generators", additional purge lines (even numbers) were introduced into which the purge lines were brought out of the "sides" of the steam generators. In the odd lines, a purge was added from the second fittings of the "pockets" of the collectors.

Modernization of the SG purge system is as follows:

- the purge pipelines from the "pockets" of the collectors and the "ends" of the steam generator are combined into one purge pipeline;
- a virtual salt compartment was identified, the concentration of dissolved substances in which is the highest, and from which a constant purge line was drawn.

At present, after all stages of modernization, the functional scheme of SG purge has the following form shown in the figure.

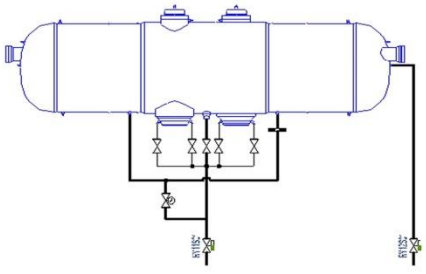

Figure 3. Scheme of continuous and periodic purge

Reconstruction of the feed water distribution system

The reconstruction of the feed water distribution system, shown in the figure, is as follows:

- the design of the feed water header was changed, 5 distribution headers were plugged from the side of the "cold" bottom of the steam generator, 4 distribution headers were added from the "hot" end and 1 distribution header was added in the area of the "cold" header;
- a partition was installed under and above the submersible perforated sheet in the area of the "cold" end 200 mm high above the submersible perforated sheet and up to the bundle of heat exchange pipes under the submersible perforated sheet;

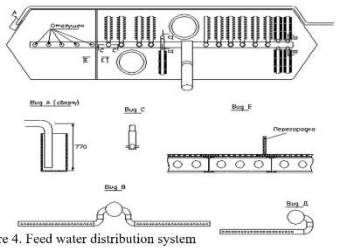

Figure 4. Feed water distribution system

Damage zone SS № 111

Another of the current problems is damage to the zone of welded joint № 111 of the "hot" (inlet) coolant collector. The damage zone is shown in the figure.

The main causes and damaging factors of damage to SS № 111 are due to a combination of the following factors:

- Corrosive environment
- Material properties
- stressed state

All damage is caused by delayed strain-corrosion cracking of the material. More ZDKR

When examining the cut template, it was concluded that the development of the crack had a staged and long-term character.

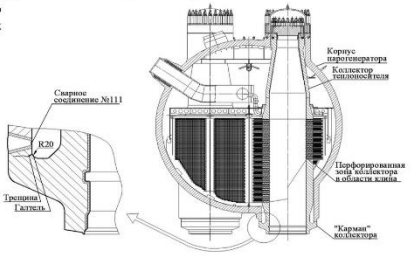

Figure 5. Steam generator PGV-1000M

From these results of the study of the ZDKR process, the following ways to prevent this process have been established

1. Reduction in the entry of corrosive impurities into SGs. Application of modern water chemistry. Reduction of copper concentration in sludge deposits. Removal of sludge from pockets, regular rinsing of pockets. Ensuring continuous purge. Line flow control. It is necessary to replace the HDPE and turbine condensers.
2. Reducing the level of tensile stresses in the metal below the yield point. To reduce tensile stresses on the fillets of the "pocket" of the collector and in the zone of the welded joint «№ 111", a method of air cooling with a temperature of 60 °C and a flow rate of 2 kg/s (6200 m3/h) of the outer layers of metal is proposed.

3D model of the method of air cooling of the zone of the welded joint № 111 of the steam generator PGV-1000M

The reduction in stress is achieved due to the temperature difference obtained as a result of cooling between the inner and outer surfaces of the pipe DN 1200, the adapter ring and the "pocket" of the collector.

It can be seen from the graph that the use of cooling of the outer surface of the pipe DN 1200, the transition ring and the "pocket" of the collector led to a decrease in tensile stresses around the entire circumference of the fillet of the "pocket" of the collector.

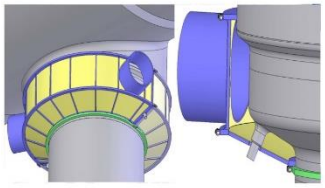

Figure 6. Design of the casing for organizing air cooling of the zone of the welded joint № 111

Graph 1. Reduction of tensile stresses around the entire circumference of the fillet of the collector pocket

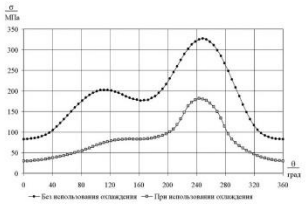

When cooling is used, the stresses in the section of the "pocket" of the collector also decrease. It can be seen from the figure that the stress over the entire fillet increased, but due to this, the stress in the zone of the welded joint decreased by about 100 MPa.

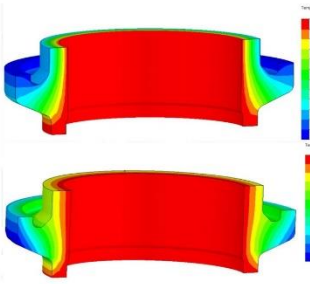

Without cooling

When coolingair

Figure 7. Temperature field in the "pocket" of the coolant collector

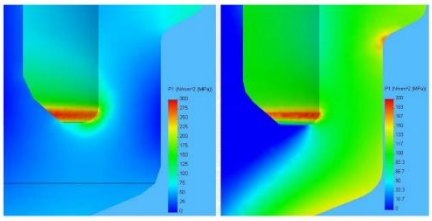

Figure 8. Stress state in the "pocket" of the collectorcoolant

The main stresses in the "pocket" of the coolant collector.

The second way to reduce tensile stresses is to create compressive forces on the DN 1200 branch pipe of the steam generator housing The slide shows a compression ring. The ring is made of steel 14X17H2, which has a lower coefficient of thermal expansion than that of the branch pipe Du 1200 of the body. This is done so that the ring compresses the pipe DN1200, gaskets are installed between the ring and the pipe; they are made of a material with a shape memory effect, this is an alloy of titanium and nickel. The wedge lock consists of half rings, a wedge, a swivel washer and a thrust washer. the figure shows the plot of the main stress in the computational domain. The maximum tensile stresses occur in the wedge lock and amount to 500 MPa. The maximum local tensile stresses in the "pocket" of the collector amounted to 240 MPa, which is 23% less than in the original version.

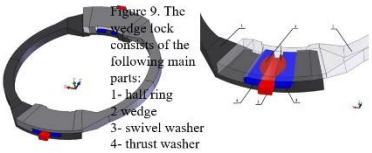

Figure 9. The wedge lock consists of the following main parts:
1- half ring
2-wedge
3- swivel washer
4- thrust washer

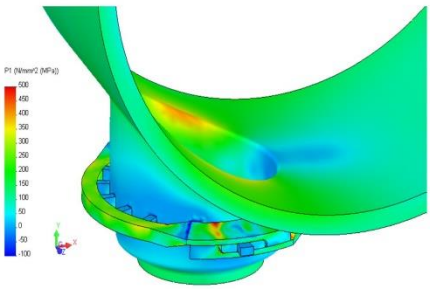

Figure 10. Diagram of the main stress in the computational domain

Conclusions

The project considered and analyzed measures to improve the reliability and ensure the resource of the steam generator PGV-1000M by modernizing the steam generator purge system.

The main causes and damaging factors for the problem of damage to collectors are identified.

Measures have been developed to reduce by 40% mechanical stresses in the area of the welded joint of the coolant header with the branch pipe Du 1200 of the SG housing, by reducing the air cooling of the zone of the welded joint № 111 .

It also shows the way to reduce tensile stresses in the fillet area of the "pocket" of the collector (the area of welded joint No. 111) by 23% by applying an external compressive force.

On this topic, I completed a graduation project at the Odessa National Polytechnic University, under the guidance of candidate of technical sciences, Associate Professor of the department of Nuclear Power Plants Oleg Alexandrovich Chulkin.

HIGH HEAT FLUX COOLING TECHOLOGY

Vojtěch SMOLÍK

Department of Energy Engineering, Faculty of Mechanical Engineering,
Czech Technical University in Prague, Prague, Czech Republic

The first wall panels of the ITER tokamak are designed for a *normal heat flux* of the order of 1-2 $MW.m^{-2}$, some panels (in the upper region of the reactor) will be required to withstand an *enhanced heat flux* up to 5 $MW.m^{-2}$. Divertor targets are components exposed to the highest heat load of 10-20 $MW.m^{-2}$. High heat flux can be cooled using the hypervapotron cooling channel geometry depicted below. Hypervaporon channel has cooling fins perpendicular to the flow of cooling liquid to intensify the heat flux from the heated wall to the cooling liquid. Subcooled boiling regime inside the hypervapotron refers to boiling from a solid surface where the bulk liquid temperature is below the saturation temperature.

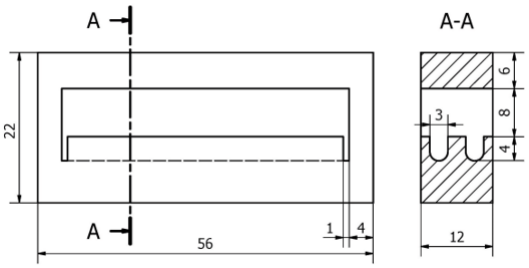

High Heat Flux Cooling Technology

Vojtěch Smolík, Master's Thesis, 2022

Department of Energy Engineering, Faculty of Mechanical Engineering, CTU in Prague

CTU
CZECH TECHNICAL UNIVERSITY IN PRAGUE

Objectives

1. Review of high heat flux cooling technology for nuclear fusion applications.
2. Simulation of subcooled boiling in hypervapotron cooling channel using ANSYS Fluent 21.2.
3. Comparison of results with other numerical analysis and experimental data.

Introduction

The first wall panels of the ITER tokamak are designed for a *normal heat flux* of the order of 1-2 MW.m^{-2}, some panels (in the upper region of the reactor) will be required to withstand an *enhanced heat flux* up to 5 MW.m^{-2}. Divertor targets are components exposed to the highest heat load of 10-20 MW.m^{-2}. High heat flux can be cooled using the **hypervapotron** cooling channel geometry (Fig. 1). Hypervaporon channel has cooling fins perpendicular to the flow of cooling liquid to intensify the heat flux from the heated wall to the cooling liquid. **Subcooled boiling** regime inside the hypervapotron refers to boiling from a solid surface where the bulk liquid temperature is below the saturation temperature.

Hypervapotron Cooling Channel Geometry

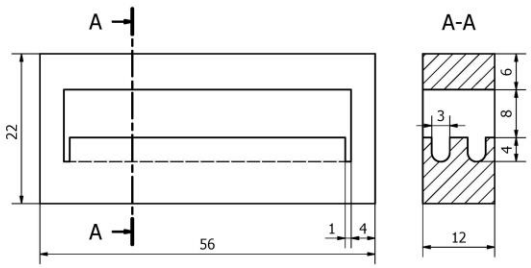

Figure 1: Box Scraper Hypervapotron Geometry [mm]

Solution

CFD solution of this thesis is based on the work of Joseph Milnes [1]. Eulerian multiphase model and $k-\varepsilon$ viscous model are selected for solution. The solution is performed on one tetrahedral and one hexahedral element type mesh. Resulting solid temperature profile (Fig. 2) is compared with eperimental data [2]. The Figure 3 shows the resulting vortex formation in hypervapotron channel. Interphase interaction is the biggest challenge of this CFD solution. Hexahedral mesh solution resulted in stable vapour layers and increased solid body temperatures (Fig. 4), tetrahedral mesh solution resulted in nearly linear heat flux/temperature relation. The boundary conditions of the solution:

Velocity Inlet :	4 m.s^{-1}	
Inlet Water Temperature :	50 °C	
Pressure Outlet :	6 bar	$\rightarrow$ $T_{saturation} = 158.83$ °C

Result: Temperature Profile

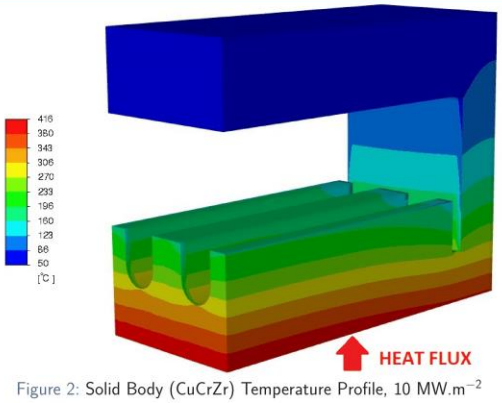

Figure 2: Solid Body (CuCrZr) Temperature Profile, 10 MW.m^{-2}

Result: Velocity Profile

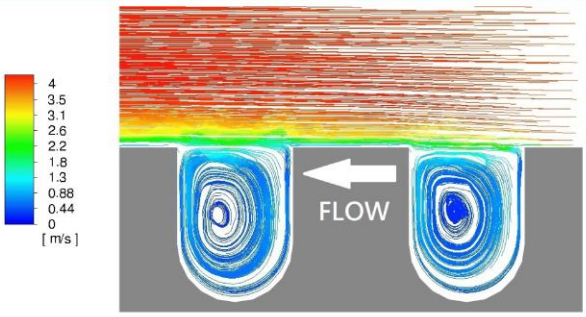

Figure 3: Vortex Formation Between The Hypervapotron Fins (Symmetry Plane)

Result: Variable Heat Flux Solution

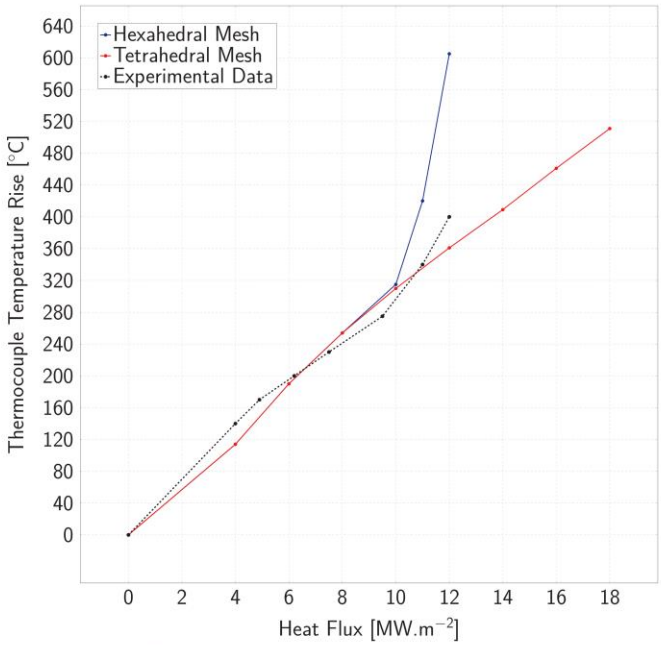

Figure 4: The Final Results of Numerical Analysis

Conclusions

- Two numerical results are presented, both fit the experimental values for low heat fluxes. For heat fluxes over 10 MW.m^{-2}: results of the tetrahedral mesh reach lower and hexahedral mesh exceed the experimental temperature data.
- More experimental results are needed to fully evaluate the quality of performed numerical solution. Experimental analysis of vapour bubble behaviour inside the hypervapotron channel can help to adjust the multiphase interaction settings to improve the accuracy of future numerical models.
- Created ANSYS Fluent 21.2 model is not able to fully simulate the subcooled boiling regime in hypervapotron conditions.

References

[1] Joseph Milnes.
Computational Modelling of the HyperVapotron Cooling Technique for Nuclear Fusion Applications.
PhD thesis, Department of Aerospace Sciences Cranfield University, Cranfield, UK, 2010.

[2] D. Ciric, M. Akiba, H.-D. Falter, D. Martin, K. Sato, and K. Yokoyama.
Design issues and fatigue lifetime of hypervapotron elements of the jet neutral beam injectors.
In *18th IEEE/NPSS Symposium on Fusion Engineering. Symposium Proceedings (Cat. No.99CH37050)*, pages 407–410, 1999.

LIQUID SALT MEASUREMENT TECHNOLOGIES

Jakub ŠPAČEK

Department of Energy Engineering, Faculty of Mechanical Engineering,
Czech Technical University in Prague, Prague, Czech Republic

Mass flow measurement is a necessary part of every nuclear reactor operation. Molten salt reactors (MSRs) are not an exception. However, the inhospitable environment somewhat complicates the process of measurement. Any such measurement in MSRs must be non-invasive which narrows down the list of applicable methods significantly. Thermal mass flow meter offers a non-invasive way of measuring flow inside a pipe via *heat transfer* while using only two very basic elements: heat source and temperature sensor. TMF using resistive heating wire and 5 temperature sensors (figure depicted below) was designed for wide range of measuring methods to experimentally find the most suitable for real life use.

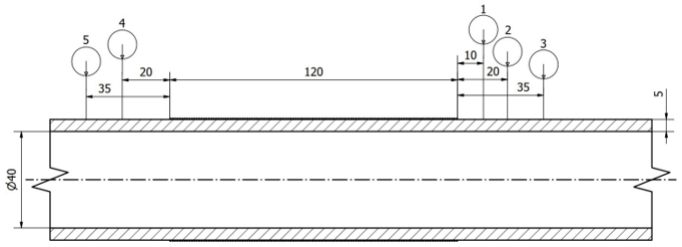

Liquid Salt Measurement Technologies

Jakub Špaček, Master's Thesis, 2022

Department of Energy Engineering, Faculty of Mechanical Engineering, CTU in Prague

CTU CZECH TECHNICAL UNIVERSITY IN PRAGUE

Objectives

1. Design of a thermal mass flow meter (TMF) for use in molten salt loops.
2. Simulation of TMF at different mass flow rates using ANSYS Fluent 2021 R2.
3. Extrapolation of correlations for measurement of mass flow inside the molten salt loop.
4. Design of scaled-down model of molten salt loop for use in school environment and potential experimental validation of TMF design.

Introduction

Mass flow measurement is a necessary part of every nuclear reactor operation. Molten salt reactors (MSRs) are not an exception. However, the inhospitable environment somewhat complicates the process of measurement. Any such measurement in MSRs must be **non-invasive** which narrows down the list of applicable methods significantly. **Thermal mass flow meter** offers a non-invasive way of measuring flow inside a pipe via *heat transfer* while using only two very basic elements: heat source and temperature sensor. TMF using resistive heating wire and 5 temperature sensors (Fig. 1) was designed for wide range of measuring methods to experimentally find the most suitable for real life use.

TMF Final Design Geometry

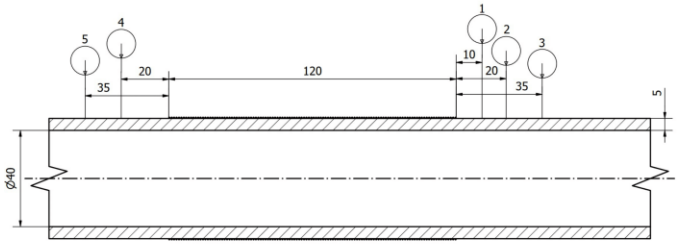

Figure 1: Thermal Mass Flow Meter Geometry

Solution

Creation of scaled model is based on work of Bardet and Peterson [1] who identified heat transfer oils as potential medium for molten salt simulation. The creation of scaled-down model is done by consecutive matching of dimentionless numbers describing desired thermohydraulic phenomena. After designing the model, comparative CFD simulation was done to verify its functionality (Fig. 3). K–omega SST viscous model is selected for all CFD simulations. Calculations are done throughout the expected mass flow range. Mass flow is defined in term of average flow velocity in the pipe. A relation of temperature on average flow velocity inside the loop is created for every measurement method (Fig. 4).

Results: Temperature Profile

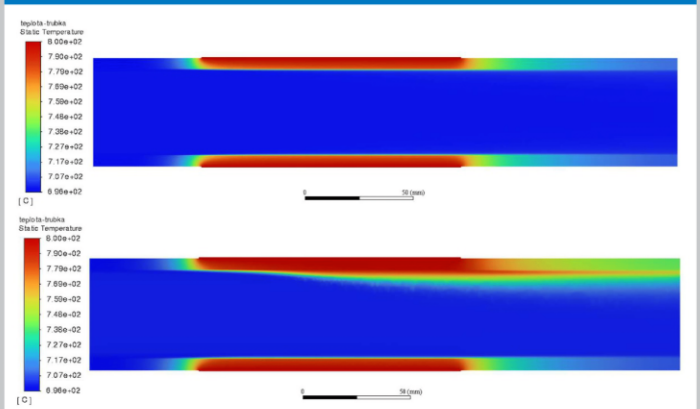

Figure 2: Heat Distribution for 0.4 [m.s^{-1}] (Top) and 0.1 [m.s^{-1}] (Bottom)

Results: Scaled-down Model Verification

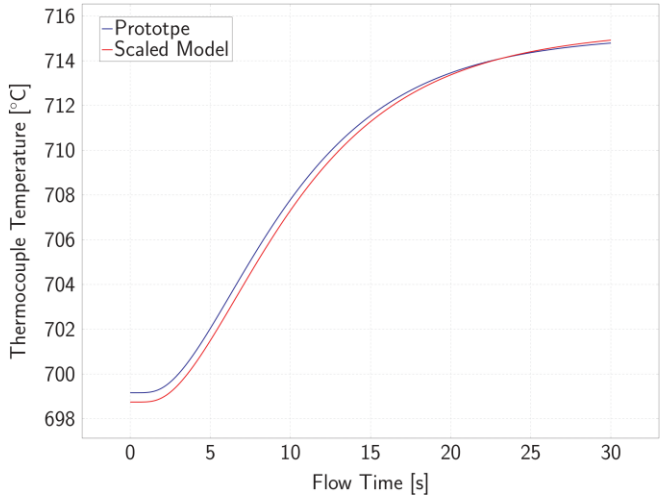

Figure 3: Comparative Transient Simulation of Scelad-down Model and Prototype

Results: Temperature Correlation

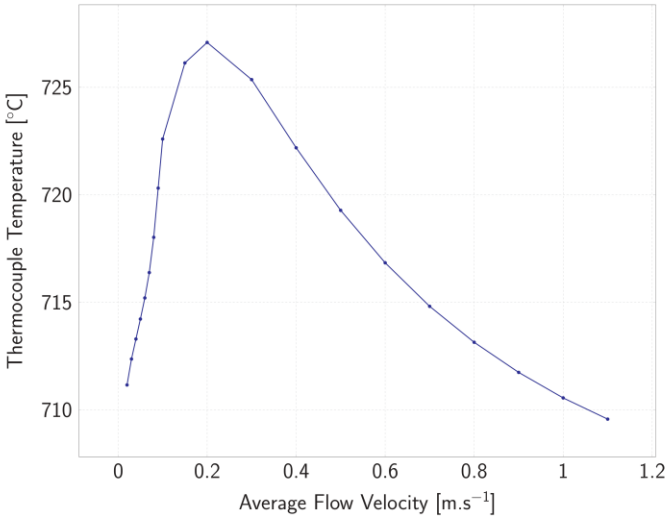

Figure 4: Example of Temperature Correlation for Steady State Measuring Method

Conclusion

- Designed TMF has many identified ways of measuring mass flow its strategically positioned temperature sensors. Each of them is suited for different measuring method with different range of measurable mass flows.
- Correlations are generally non-linear and their trends change when transitioning from laminar to turbulent flow.
- Simulation fluid and operational parameters of a scaled-down loop suitable for school environment have been identified. Model loop is roughly half the size of the prototype, uses heat transfer oil (Therminol 72) instead of FLiBe salt and requires only 1 % of heating and pumping power. Simulation showed good ability of the scaled-down system to copy thermohydraulic behavior of the prototypical molten salt loop.

References

[1] Philippe M. Bardet; Per F. Peterson.
Options for scaled experiments for high temperature liquid salt and helium fluid mechanics and convective heat transfer.
In *Nuclear Technology*, volume 163:3, page 344–357, 2008.

AN ENERGY PATHWAY TO ACHIEVE CARBON NEUTRALITY IN FRANCE BY 2050

Ashith VALLERIYAN

ENSTA Paris, Institut Polytechnique de Paris, Paris, France

While nuclear account for about 70% of the electricity produced in France, it represents less than 20% of final energy used in the country. About 40% of the energy used in France is from petroleum products and the rest is natural gas (about 20%). As a result, achieving carbon neutrality will require phasing out nearly all of this fossil fuel energy. A single 1,000 megawatt nuclear reactor could produce more than 150,000 tonnes of hydrogen each year. I propose to increase the share of primary energy generated by nuclear power by producing hydrogen gas which can then be used as fuel (substitute for natural gas) for industrial and transport purposes.

Master of Nuclear Energy
ENSTA Paris | Institut Polytechnique de Paris
828 boulevard des Maréchaux
91120 Palaiseau, France.
ashith.valleriyan@ensta-paris.fr

AN ENERGY PATHWAY TO ACHIEVE CARBON NEUTRALITY IN FRANCE BY 2050

Ashith VALLERIYAN

Date : 4th July 2022

ABSTRACT :

- While nuclear account for about 70% of the electricity produced in France, it represents less than 20% of final energy used in the country. [1]
- About 40% of the energy used in France is from petroleum products and the rest is natural gas (about 20%) [1]
- As a result, achieving carbon neutrality will require phasing out nearly all of this fossil fuel energy.
- A single 1,000 megawatt nuclear reactor could produce more than 150,000 tonnes of hydrogen each year.[2]
- I propose to increase the share of primary energy generated by nuclear power by producing hydrogen gas which can then be used as fuel (substitute for natural gas) for industrial and transport purposes.

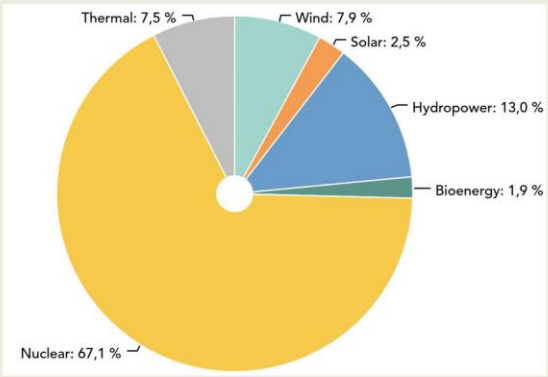

RTE Electricity Report of France - 2020 [3]

INDUSTRIAL CONTEXT

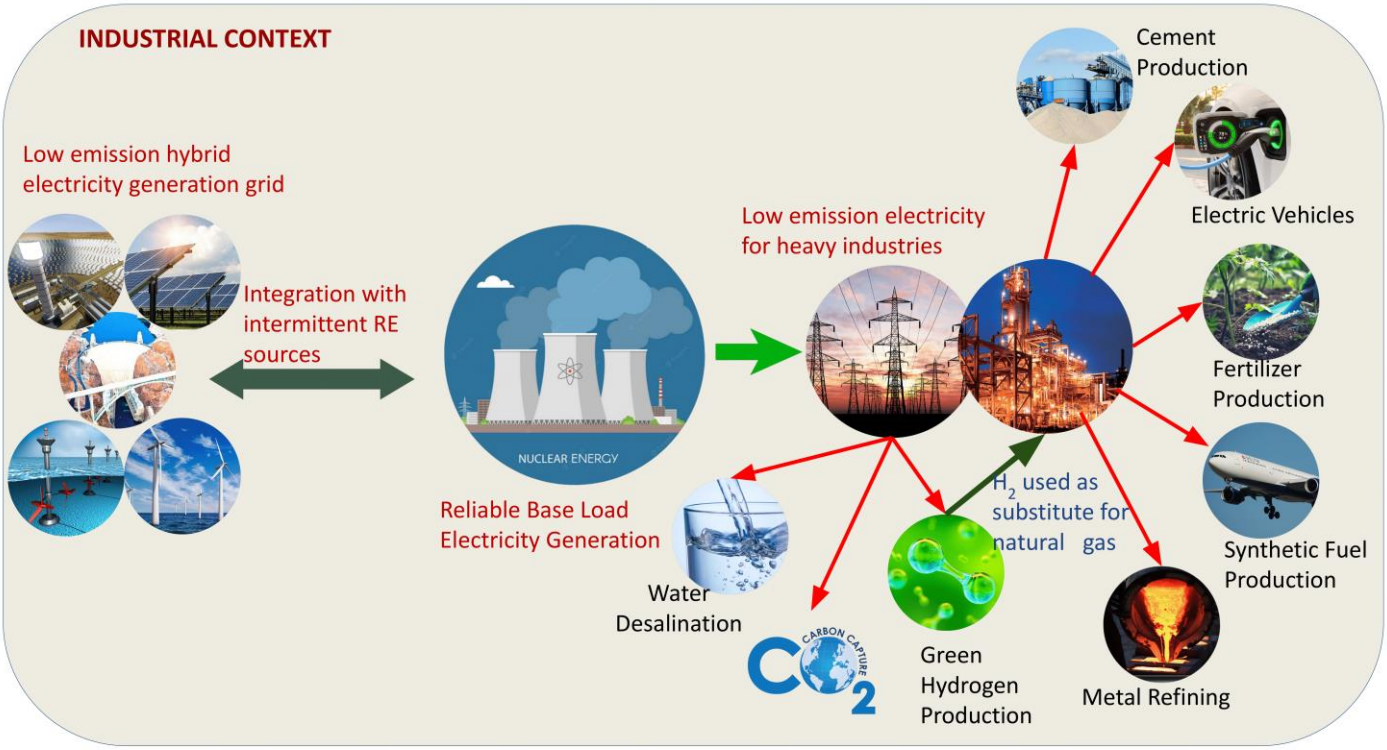

CONCLUSION & PERSPECTIVES

- The current energy crisis shows that phasing out fossil fuels is not only imperative for the climate; it is also a reminder that Europe's heavy reliance on hydrocarbon-producing countries can come at an economic cost and energy dependence.
- Nuclear futures will likely include markets beyond baseload electricity like H_2 generation. H_2 can then be used for non-energy and indirect energy purposes as well as used directly as a fuel, helping to achieve carbon neutrality by 2050.
- Nuclear hydrogen can be exported to neigbouring countries like germany through existing pipelines meant to carry natural gas with slight modification, creating revenue for the nuclear sector. This also improves the energy independence of Europe.

REFERENCES

1. Energy pathways to 2050 - Key results by RTE, October 2021
2. Office of Nuclear Energy, US Department of Energy. https://www.energy.gov/ne/articles/could-hydrogen-help-save-nuclear
3. RTE Electricity Report of France - 2020 [3]

Ph.D. STUDENTS

OPTIMIZATION OF NUCLEAR DRIVEN DISTRICT HEAT SUPPLY

Hussein Abdulkareem Saleh ABUSHAMAH

Faculty of Electrical Engineering, University of West Bohemia, Pilsen, Czech Republic

Space and water heating are responsible for about 78% of the total residential sector energy consumption in the EU, of which about 40% is supplied by natural gas (NG) driven systems. These days the price of natural gas in the EU is souring, confirming that NG could not be a reliable energy source anymore from an energy policy viewpoint. Furthermore, carbon emission is one of the vital aspects of energy supply planning, and NG has average CO_2 emissions of 185 kg per MWh. Therefore, integrating heat-only SMRs such as Teplator with auxiliary systems heat storage and boilers (peak shaving and flexible load following) is eligible to be a competitive scenario. Here, optimizing the required capacities and operation scheduling of the units is formulated and evaluated.

Optimization of Nuclear Driven District Heat Supply

Hussein Abdulkareem Saleh Abushamah[1] abushama@fel.zcu.cz

[1] Faculty of Electrical Engineering, University of West Bohemia, Pilsen, Czech Republic.

NUCLEAR DAYS ZČU v Plzni 14.9. – 19.10. 2022

FACULTY OF ELECTRICAL ENGINEERING UNIVERSITY OF WEST BOHEMIA

Introduction

Space and water heating are responsible for about 78% of the total residential sector energy consumption in the EU, of which about 40% is supplied by natural gas (NG) driven systems [1]. These days as illustrated in Fig. 1, the price of natural gas in the EU is souring, confirming that NG could not be a reliable energy source anymore from an energy policy viewpoint. Furthermore, carbon emission is one of the vital aspects of energy supply planning, and NG has average CO2 emissions of 185 kg per MWh [3]. Therefore, integrating heat-only SMRs such as Teplator with auxiliary systems heat storage and boilers (peak shaving and flexible load following) is eligible to be a competitive scenario. Here, optimizing the required capacities and operation scheduling of the units is formulated and evaluated.

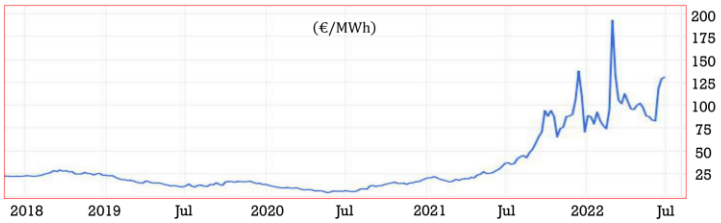

Fig. 1: Natural Gas EU Dutch TTF [2].

Fig. 2 illustrates a simple drawing of the idea, and the assumed hourly heat demand is created from typical buildings' heat consumption profile [4]. Table. 1 addresses the considered parameters, some extracted from [5, 6, 7] and some are assumptions.

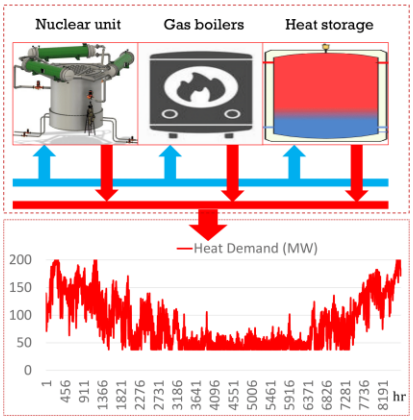

Fig. 2: District heat supply system and the hourly heat demand profile.

Table 1: Assumed parameters [5, 6, 7]

parameters	Tep	Gb	HS
DMP	50 years		
Lifetime (LT) (yr)	50	25	50
Shutdown (d/yr)	30	0	0
Power ramp rate (%R)	%10	%100	%10
Investment cost	30 M€/150 MW	60 k€/MW	3 k€/MWh
Fixed O&M per yr	12 M€/150 MW	2 k€/MW	8.6 €/MWh
Variable O&M cost	1.1 €/MWh	1.1 €/MWh	0 €/MWh
Fuel cost €/MWh	0	80	0

Formulations

According to the equations given in Table. 2, the economic model is based on the present value of the annual cash flow. 2. The objective function is determined to minimize the system's total construction and operation cost. The specific heat generation cost (SHGC) includes the fuel cost, variable operation and maintenance cost, and carbon emission cost per MWh of heat generation.

Table 2. Economic Equations

Overnight Investment Cost (C_{PV}^{I}) C: Capacity SIC: Specific Investment Cost	$C_{PV}^{I}\ (€) = SIC(€/\mathrm{MW}) \times C(MW)$
Annual Heat Generation Cost (AHGC) SHGC: Specific Heat Generation Cost	$\mathrm{AHGC}\ (€) = \sum_{i=1}^{8760} HG^{i} \times SHGC\ (€/\mathrm{MWh})$
Reconstruction Cost (RC) after each lifetime (along decision making period (DMP))	$C_{PV}^{RB}(€) = R\,C/(1+r)^{LT}$
Annual Maintenance Cost ($/MW/year) SMC: Specific maintenance cost	$AMC(€) = C \times SMC(€/MW/yr)$
Objective Function: The present value of the total cost (C_{PV}^{Tot}), r: Interest rate	$C_{PV}^{Tot}\ (€) = C_{PV}^{I} + C_{PV}^{RB}(€) + (AHGC\ (€) + AMC) \sum_{n=1}^{DMP} \frac{1}{(1+r)^{n}}$

The optimization program searches for the optimum solution which satisfies the technical constraints. The technical constraints are given in Table. 3. For example, the energy balance must be satisfied. The hourly heat generation must be within the nominal power of the units considering their capability of decreasing or increasing the output power. One month of maintenance and refuelling process is assumed for the nuclear unit, and this shutdown period is included in the optimization. The charging/discharging scheduling of the heat storage must comply with its nominal capacity and input/output power rate.

Table 3. Technical Constraints

Energy balance HD: heat demand. HG: heat generation	$HD^{i} = HG_{Tep}^{i} + HG_{Gb}^{i} + CD_{Hs}^{i}$
Complying with capacity of heat generation $Cp\ (MW)$: thermal power capacity	$HG_{Tep}^{i} \le Cp_{Tep}, \quad HG_{Gb}^{i} \le Cp_{Gb}$
Complying with power change rate R (%): power change per hour	$HG_{U}^{i-1} - Cp_{U}.R_{U} \le HG_{U}^{i} \le HG_{U}^{i-1} + Cp_{U}.R_{U}$, $i=2,3,\ldots,8640$ U: Teplator, Gas boiler
Shutting down the nuclear unit during annual maintenance and refueling period	$HG_{Tep}^{i}=0, \quad i=5000-5720$ (one month in summer)
The stored heat on hour (i)	$SE_{Hs}^{i} = SE_{Hs}^{i-1} - CDC_{Hs}^{i}{}^{i-1}$, i=2, 3, 4, ..., 8640
Discharged heat must not exceed the stored heat during discharging.	$CDC_{Hs}^{i} \le SE_{Hs}^{i}$, Discharging, $CDC_{Hs}^{i} > 0$
Charged heat must not exceed the free capacity of the heat storage during charging.	$-CDC_{Hs}^{i} \le Cp_{Hs} - SE_{Hs}^{i}$, Charging, $CDC_{Hs}^{i} < 0$
Charging and discharging per hour must comply with the nominal rates.	$-R_{Hs}^{ch} \le HG_{Hs}^{i} \le R_{Hs}^{dch}$

Results and Conclusions

The optimum design capacities are given in Table. 4, and the optimum operation scheduling is illustrated in Fig. 3. The nuclear source is the main heat generator, and the gas boiler only is operated during the shutdown period of the nuclear source and for some peak shaving points. While the peak demand is 225 MW, the installed generation capacity is 185.5 MW. Heat storage effectively contributed to the flexible load following and cost and generation capacity savings. The annual demand is 737 GWh, of which 707 GWh is supplied by nuclear energy, saving about 96% of the carbon emissions. Consequently, the results confirm the techno-economic feasibility and emissions-saving of the nuclear district heating system.

Table 4. Optimum design capacities

Unit	Capacity
Teplator (one unit)	150 MW
Heat Storage	6,333 MWh
Gas Boiler	35.54 MW
Present value of total cost (50 years DMP)	143 M€

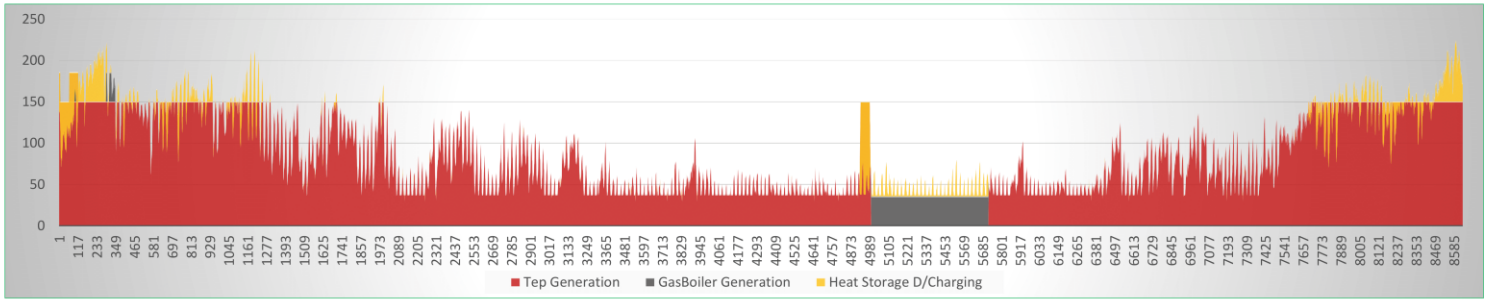

Fig. 3: Optimized heat generation scheduling of the nuclear heating reactor (Teplator), gas boilers, and heat storages.

References:

[1] Energy consumption in households - European Commission.

[2] EU natural gas, tradingeconomics.com

[3] www.carbonindependent.org/files/conversion-factors.pdf

[4] Yilmaza, Selin, et al. Hourly Demand Profiles for Space Heating and Electricity. ETH Zurich, 2020.

[5] Skoda, Radek, et al. "TEPLATOR: nuclear district heating solution." (NENE), Portoroz, Slovenia, September. 2020.

[6] Technology Data Catalogue for Electricity and district heating production - March 2022, DE Authority.

[7] Technology data for energy storage, updated 2020, DE Authority.

Acknowledgment: This work was supported by the UWB [SGS- 2021-018] and Czech technological agency [TK 03030109].

SORPITON OF EUROPIUM ON CEMENTITIOUS MATERIALS IN THE PRESENCE OF ORGANIC SUBSTANCES

Marta BUREŠOVÁ, Barbora DRTINOVÁ, Jana KITTNEROVÁ

Czech Technical University in Prague, Prague, Czech Republic

In order to assess the safety of low and intermediate level waste repositories and deep geological repositories for spent nuclear fuel, it is necessary to describe the behaviour of stored radionuclides. The study focuses on europium, known as a chemical analogue of trivalent actinides, in particular Am (III) and Cm (III). The migration of radionuclides is affected by sorption on the material of the engineering barriers of the repositories, including cement-based barriers. Radionuclides can interact not only with the filling of barrels with low and intermediate level waste and concrete containers, but the issue also concerns the structural elements of repositories. Present organic substances either as a part of the waste (plastics, rubber, cellulose or for example ion exchange resins) or as additives improving properties of cementitious materials can also significantly affect the transport of radionuclides. Specifically for Eu, a significant reduction of the sorption on cement due to the presence of organic ligands and cement additives at concentrations expected in fresh cement and technical grade concrete can occur. Radionuclide sorption is described by the distribution ratio (R_d) between the liquid and solid phases (L/S) or by sorption isotherm.

Sorption of europium on cementitious materials in the presence of organic substances

Marta Burešová, Barbora Drtinová, Jana Kittnerová
Czech Technical University in Prague, Břehová 7, 115 19 Prague 1, Czech Republic
Corresponding Author, E-mail: buresma8@fjfi.cvut.cz

Introduction

In order to assess the safety of low and intermediate level waste repositories and deep geological repositories for spent nuclear fuel, it is necessary to describe the behaviour of stored radionuclides. The study focuses on europium, known as a chemical analogue of trivalent actinides, in particular Am (III) and Cm (III). The migration of radionuclides is affected by sorption on the material of the engineering barriers of the repositories, including cement-based barriers. Radionuclides can interact not only with the filling of barrels with low and intermediate level waste and concrete containers, but the issue also concerns the structural elements of repositories. Present organic substances either as a part of the waste (plastics, rubber, cellulose or for example ion exchange resins) [1] or as additives improving properties of cementitious materials can also significantly affect the transport of radionuclides. Specifically for Eu, a significant reduction of the sorption on cement due to the presence of organic ligands and cement additives at concentrations expected in fresh cement and technical grade concrete can occur [2]. Radionuclide sorption is described by the distribution ratio (R_d) between the liquid and solid phases (L/S) or by sorption isotherm.

Materials

Solid phase

- Hardened cement paste
  - HCP CEM I (fraction ≤ 0.4 mm)
  - HCP CEM III (fraction ≤ 0.5 mm)
- Calcium – Silicate – Hydrates (CSH) Ca/Si = 1

Liquid phase

- Portlandite water (saturated $Ca(OH)_2$ solution for cements)

Methods

Sorption under different conditions

- Liquid to solid phase ratios (L/S 100-1000 L kg^{-1})
- Addition of organic substances (adipic acid (AD), phthalic acid (PH), EDTA) with different concentration (5·10^{-3} and 5·10^{-5} mol L^{-1} selected on the basis of the report [3])

Measurement: HPGe gamma detector

Evaluation

Distribution ratio: $R_d = \frac{A_0 - A_t}{A_t} \cdot \frac{V}{m}$

K_d-model for linear isotherm: $q = K_d \cdot c$

Langmuir isotherm: $q = \frac{K_L \cdot c \cdot Q_{max}}{1 + K_L \cdot c}$

A_0(Bq) is the initial activity of the radionuclide in solution, A_t(Bq) is the activity at the time t, V (L) is the volume of the liquid phase, m (kg) is the mass of solid phase used in the experiment, q (mol kg^{-1}) is the equilibrium concentration in the solid phase, c (mol L^{-1}) is equilibrium concentration in the liquid phase and K_d (L kg^{-1}) is the distribution coefficient, dimensionally identical to the distribution ratio R_d, K_L (L mol^{-1}) is the equilibrium constant of the addition reaction and Q_{max} (mol kg^{-1}) is the maximum achievable concentration of the monitored component in the solid phase.

Results

Kinetic sorption experiments

For all experiments equilibrium is reached within 24 hours. Accordingly, the sampling time for the equilibrium experiments was set at 48 hours.

Results

Equilibrium sorption experiments

- The influence of the presence of organic substance on the value of R_d was clearly indicated
- The R_d were in the tens of thousands (L kg^{-1}) which is in agreement with the R_d values of americium [4]

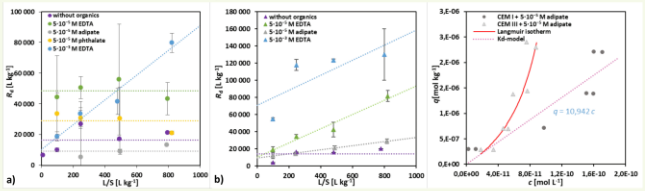

Fig.1: a) Distribution ratios of ^{152}Eu sorption on CEM I under different conditions. b) Distribution ratios of ^{152}Eu sorption on CEM III under different conditions (Fitted trends are added for greater clarity). c) Linear sorption of Eu on HCP CEM I with the addition of AD fitted with K_d-model and Langmuir isotherm of sorption of Eu on HCP CEM III with the addition of AD

- For HCP CEM I without organic substances and with the addition of AD, PH, EDTA at a concentration of 5·10^{-5} mol L^{-1} and for HCP CEM III without organic substances the dependence of R_d on L/S was not observed – evaluated using the K_d-model

Tab. 1: Values of distribution coefficients K_d determined using K_d-model and average R_d values for studied systems

System	Average R_d [L kg^{-1}]	K_d [L kg^{-1}]
HCP CEM I without organic	16,472 ± 3,078	19,567 ± 1052
HCP CEM I EDTA 5·10^{-5} mol L^{-1}	48,604 ± 9,083	32,125 ± 5597
HCP CEM I AD 5·10^{-5} mol L^{-1}	9,274 ± 1,733	10,942 ± 1044
HCP CEM I PH 5·10^{-5} mol L^{-1}	29,080 ± 5,434	17,463 ± 2746
HCP CEM III without organic	14,111 ± 3,585	15,384 ± 2296

- For HCP CEM I with the addition of EDTA at a concentration of 5·10^{-3} mol L^{-1} and for HCP CEM III with the addition of EDTA at a concentration of 5·10^{-3} mol L^{-1} and AD at a concentration of 5·10^{-5} mol L^{-1} the dependence of R_d on L/S was observed – evaluated by Langmuir isotherm
- In the HCP CEM III EDTA 5·10^{-5} mol L^{-1} system, the R_d depends on L/S, no suitable interpolation using the Langmuir isotherm was found

Tab. 2: Parameters of Langmuir isotherm for different systems and determined range of R_d values

System	R_d [L kg^{-1}]	K_L [L mol^{-1}]	Q_{max} [mol kg^{-1}]
HCP CEM I EDTA 5·10^{-3} mol L^{-1}	18,860-79,792	-1.90E+10	-9.20E-07
HCP CEM III EDTA 5·10^{-3} mol L^{-1}	55,135-130,232	-2.40E+10	-3.00E-06
HCP CEM III AD 5·10^{-5} mol L^{-1}	12,325-28,992	-7.29E+9	-1.34E-06
HCP CEM III EDTA 5·10^{-5} mol L^{-1}	19,331-81,794	-	-

Conclusion

Kinetic sorption experiments demonstrated that sorption of europium on cementitious materials occurs very quickly, and equilibrium is reached within 24 hours under all studied conditions. Considering the experimental errors, we can only conclude that the distribution ratios are in the order of 10^3-10^5 L kg^{-1} for Eu sorption on both CEM I and CEM III materials, which is in agreement with the R_d values for americium. The type and concentration of organic substance affect the R_d values differently. Ambiguous effect on the shape of isotherms caused by addition of organic substances will be further studied.

Reference

[1] IAEA, 'Predisposal Management of Organics in Radioactive Waste', 2004.
[2] M. Dario, B. Allard, and S. A. Kärnbränslehantering, 'Effect of organic ligands on the sorption of europium on TiO_2 and cement at high pH', vol. 270, no. 3, pp. 495–505, 2004.
[3] L. VanLoon and W. Hummel, 'The radiolytic and chemical degradation of organic ion exchange resins under alkaline conditions: Effect on radionuclide speciation', no. 95–08, p. 112, 1995.
[4] M. Ochs, D. Mallants, and L. Wang, 'Radionuclide and Metal Sorption on Cement and Concrete', vol. 9999, pp. 171–182, 2015.

Acknowledgment

The research leading to these results has received funding from the European Union's Horizon 2020 Innovation Programme under grant agreement n° 847593 (EURAD – CORI). The output was created with financial participation of SÚRAO (Czech Radioactive Waste Repository Authority) (SO2020-017). This contribution is also partially a result of the grant of the CTU Student Grant Scheme No. SGS22/187/OHK4/3T/14.

CFD BENCHMARK FOR THE SINGLE FPFA FUEL ASSEMBLY FOR REACOR LVR-15

Štěpán HROUDA, Jan SYBLÍK, Miroslav GLEITZ, Michal CIHLÁŘ

Department of Energy Engineering, Czech Technical University in Prague,
Prague, Czech Republic

Uranium fuel for research reactors FPFA Flat Plate Fuel Assembly was developed by Technic Atome and manufactured by Framatome-CERCA in France. In this work, CFD simulations (ANSYS Fluent and StarCCM+) of the flow characteristics through an FPFA and subsequent verification of the results in an experimental loop on the fuel model were performed.

Water with a temperature of 15 °C to 50 °C and a mass flow rate of up to 12 kg/s flowed through the FPFA fuel assembly. The flow was measured with a GE AT600 ultrasonic flow meter. The pressure was measured with a Rosemount 10 mm differential pressure transducer in front of and behind the fuel model. Temperature was measured with K-type thermocouples in the test zone before and after the fuel model and in the water tank.

CFD Benchmark for the Single FPFA Fuel Assembly for Reactor LVR-15

authors: Štěpán Hrouda[a,*] Jan Syblík[a], Miroslav Gleitz[a], Michal Cihlář[a]
[a]Department of Energy Engineering, Czech Technical University In Prague, Technicka 1902/4, 160 00 Prague, Czech Republic
[*]Corresponding author: stepan.hrouda@fs.cvut.cz

FPFA Fuel for the First Time in an LVR-15 Reactor

Uranium fuel for research reactors **FPFA** **F**lat **P**late **F**uel **A**ssembly was developed by **Technic Atome** and manufactured by **Framatome-CERCA** in France.

In this work, CFD simulations (**ANSYS Fluent** and **StarCCM+**) of the flow characteristics through an FPFA and subsequent verification of the results in an experimental loop on the fuel model were performed. Water with a temperature of 15 °C to 50 °C and a mass flow rate of up to 12 kg/s flowed through the FPFA fuel assembly. The flow was measured with a **GE AT600 ultrasonic flow meter**. The pressure was measured with a **Rosemount** 10 mm differential **pressure transducer** in front of and behind the fuel model. Temperature was measured with **K-type thermocouples** in the test zone before and after the fuel model and in the water tank.

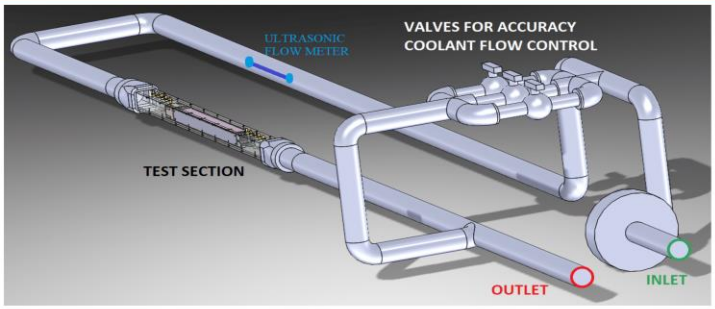

Comparison of Experimental and Computed Data

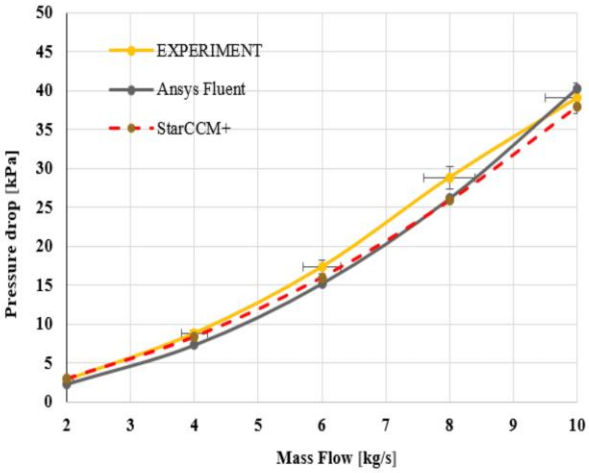

The graph shows a comparison of the pressure drop at a water temperature of 50 °C. The **yellow curve** is the pressure drop obtained from the **measurement**. The **black curve** is the simulation in **ANSYS Fluent** and the **red curve** is the CFD simulation in **StarCCM+**.

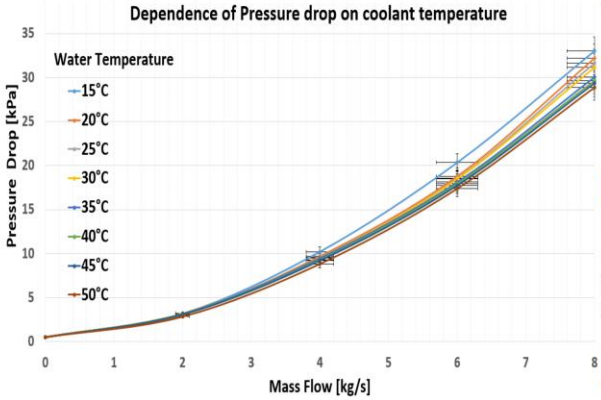

Mass flow [kg·s^{-1}]	Flow [kg·s^{-1}]	Pressure [kPa]	Temperature [°C]
2	±0.09	±0.77	±1.23
4	±0.14	±0.78	±1.23
6	±0.09	±0.78	±1.23
8	±0.22	±0.79	±1.23

Original IRT-4M and Successoring FPFA Fuel

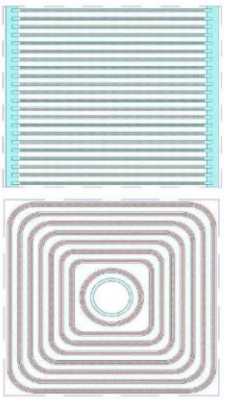

The main difference between **IRT-4M** and **FPFA** fuel is in **geometry** and **matrix** type. **Matrix type IRT-4M is UO_2** against **FPFA is U_3Si_2**. IRT-4M has 8 fuel concentical elements with **total weight of Uranium 300 g.** FPFA has 22 flat plate elements with a total weight of Uranium 384 g. The **enrichement** in both cases **is 19.75 %**. The fuel assemblies have an overall different design.

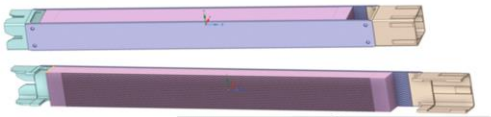

Surface Roughness Approximation

Surface roughness was measured by INSIZE ISR-C300 roughness meter. Surface profile can be seen in figure below. Roughness Average (**Ra**) **0.44 µm** and Maximum Peak (**Ry**) or Mean Roughness (**Rz**) **4.63 µm**. In CFD was surface defined by parameters **roughness height** and **roughness constant** (value 0.5 was used). Roughness height was determined according by the measurement.

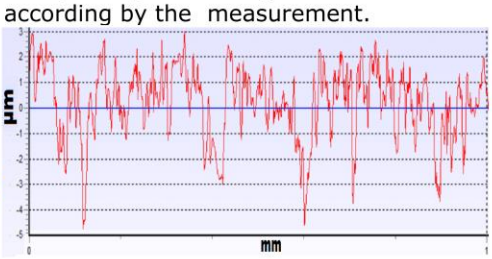

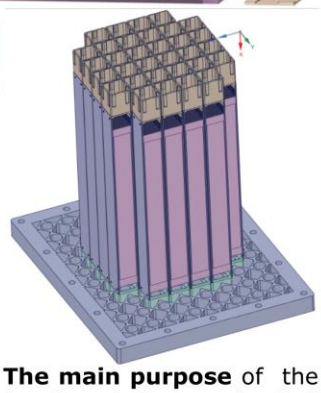

The main purpose of the benchmark is to make **full core CFD simulation,** (consists of **32 fuel assemblies** and 12 of them are controling) based on validated parameters obtained from single fuel assembly.

Uncertainty Measurement

Uncertainties were determined according to **ISO 15189.** The uncertainty of **flow** and **pressure** measurements **depends on mass flow**. The uncertainty of the **temperature is constant**. The uncertainty values can be seen in the table below-left.

Conclusion

Simulated data are in range of measurement uncertainties, in average deviation **-12.4%** for **Ansys Fluent**, **5.2%** for **StarCCM+**, which means current model settings can be applied on full core model.

Read More:

INVESTIGATION OF HEAT TRANSFER IN THE ANNULAR CHANNEL AROUND THE HEATED WALL OF THE FUEL ROD

Petr KLAVÍK

Faculty of Mechanical Engineering, University of West Bohemia, Pilsen, Czech Republic

The presented paper focuses on heat transfer research on a fuel rod model in the area of the spacer grid. The simulation of the flow field and a heat flux from the model of the fuel rod was performed on the experimental measuring track. The goal of the study was to find the critical heat flux for a specific geometry and given input values of the coolant flow rate.

During the operation of the pressurized water reactor, a sufficient heat removal from the fuel to the coolant must be ensured. At the same time ensure the flow of subcooled coolant below the lower saturation limit (ensured only a single-phase coolant flow). This text focuses on the issues of a heat transfer during two-phase flow in a channel. The vapor component contained in the coolant stream significantly reduces heat transfer from the cooled wall. The result is an increase in wall temperature. This phenomenon known as boiling crisis can result in permanent damage to the material/wall surface. The article also deals with the measurement of the fuel rod model on the experimental measuring track that was built for this research.

INVESTIGATION OF HEAT TRANSFER IN THE ANNULAR CHANNEL AROUND THE HEATED WALL OF THE FUEL ROD

Petr Klavík
University of West Bohemia
ŠKODA JS a.s. petr.klavik@skoda-js.cz

NUCLEAR DAYS

FACULTY OF MECHANICAL ENGINEERING
UNIVERSITY OF WEST BOHEMIA

ŠKODA JS

Abstract

The presented paper focuses on heat transfer research on a fuel rod model in the area of the spacer grid. The simulation of the flow field and a heat flux from the model of the fuel rod was performed on the experimental measuring track. The goal of the study was to find the critical heat flux for a specific geometry and given input values of the coolant flow rate.

Introduction

During the operation of the pressurized water reactor, a sufficient heat removal from the fuel to the coolant must be ensured. At the same time ensure the flow of subcooled coolant below the lower saturation limit (ensured only a single-phase coolant flow). This text focuses on the issues of a heat transfer during two-phase flow in a channel. The vapor component contained in the coolant stream significantly reduces heat transfer from the cooled wall. The result is an increase in wall temperature. This phenomenon known as boiling crisis can result in permanent damage to the material/wall surface. The article also deals with the measurement of the fuel rod model on the experimental measuring track that was built for this research.

Critical heat flux

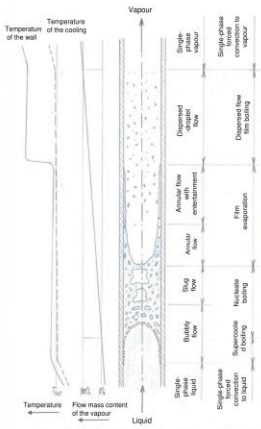

FIG. 1 – Example of classification of two-phase flow in the vertical channel.

The water subcooled below the lower saturation limit enters the active zone in the pressurized water reactors. The heating of the coolant is caused by the transfer of the heat from the surface of the fuel rods. Conditions for a heat transfer crisis begin when the weight amount of the steam in the coolant increases above the permissible limit. The development of a heat transfer crisis in a two-phase flow is caused by a random phenomena in the boiling mechanism. The main effect is a sudden increase in the temperature of the surface through which the heat is transferred. This change in the boiling mechanism is primarily due to reaching the saturation temperature on the heated wall and instabilities in the coolant flow. After saturation is reached, a nucleate boil occurs, which turns into a developed membrane-like boil over the entire flow cross section. Oscillations in the coolant stream cause pressure and velocity changes. These local changes directly affect the temporary decrease the pressure and the resulting increase in liquid overheating in that location. Along with overheating of the liquid, the extent of evaporation also increases. The temperature of the wall surface is significantly higher than the temperature of the liquid and the direct contact of the liquid with this surface is interrupted. Evaporation further takes place through the vapor layer, resulting in a significant reduction in heat transfer and a decrease in the cooling efficiency of the heated wall. The temperature of the heated wall increases up to values at which its material is permanently damaged. This mode of heat removal is unallowable during the operation of a nuclear reactor.

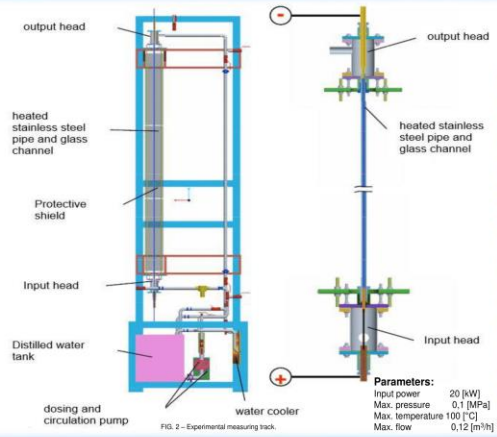

FIG. 2 – Experimental measuring track.

Experimental measuring track

The experimental measuring track was designed to investigate the heat transfer crisis on a single-rod and a multi-rod model of a fuel rod at a dimensional scale of 1:1. An experimental measuring track consists of a water circuit, a DC electrical source, a model of a fuel rod, control and measuring equipment. After the test measurement a Watson-Marlow peristaltic pump is newly placed for the precise setting of the constant flow without pressure pulsations. Distilled water is used as the cooling liquid. The main part of the entire device is the measuring channel, which consists of a glass tube, an inlet head, an outlet head, a model of a fuel rod and a sliding device for traversing the thermocouple probe. The model of a fuel rod is inserted into a glass tube and fixed in the heads. The heads are used not only for fixing, but also for connecting electrodes from the DC electrical source, directing the coolant flow at the entrance to the channel, and temperature and pressure measurements. There is also a heat exchanger to ensure a constant temperature of the coolant in the tank even during a long measurement. Measurement processes, control of sub-components or data processing and storage are secured by a purpose-built program in the NI LabVIEW graphical programming environment.

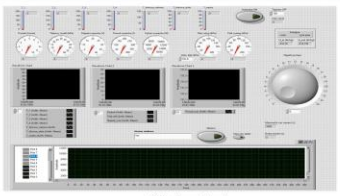

FIG. 5 – The control panel.

FIG. 3 – Peristaltic pump.

FIG. 9 – The spacer.

FIG. 7 – The thermocouple probe.

FIG. 4 – Rod-electrode connection.

FIG. 6 – The thermocouple probe.

FIG. 8 – The model of fuel rod.

FIG. 10 – Part of the track.

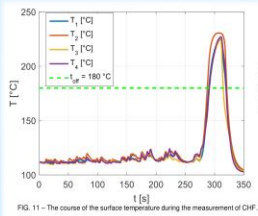

FIG. 11 – The course of the surface temperature during the measurement of CHF.

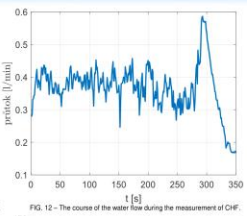

FIG. 12 – The course of the water flow during the measurement of CHF.

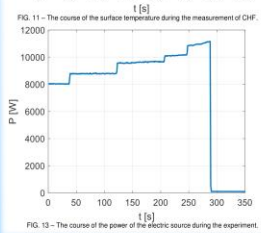

FIG. 13 – The course of the power of the electric source during the experiment.

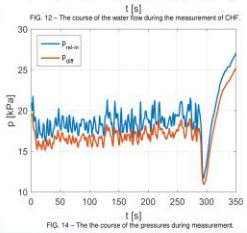

FIG. 14 – The the course of the pressures during measurement.

Results

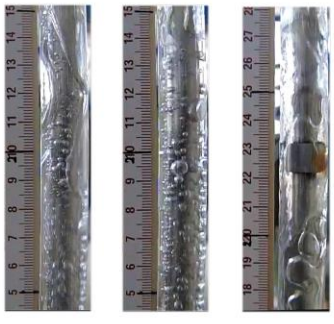

FIG. 17 – Illustrative example of the optical recording of the boiling process (selected moments of the camera recording at 300 fps).

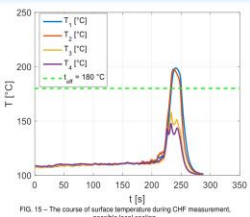

FIG. 15 – The course of surface temperature during CHF measurement, possible local cooling.

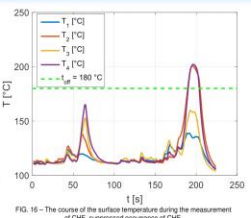

FIG. 16 – The course of the surface temperature during the measurement of CHF, suppressed occurrence of CHF.

The critical heat flux is characterized by a sharp increase in the surface temperature of the heated rod. This phenomenon is captured in the figure 11 for all four thermocouples inserted inside the rod at the same height but at different places around the perimeter. In the figures 15 and 16 we present an example where some thermocouples show a sharp rise in the temperature up to the point of switching off the power source at 180 °C and some detect possible local cooling.

Conclusion

The presented study investigated the finding of the critical heat flux on the created model of a fuel rod under given boundary conditions. The first measurement on the experimental device made it possible to map the temperature field on the inner wall of the rod model, not only in the area of the spacer grids. Further measurement results will be used to validate CFD numerical simulations of the same task. Further analysis will focus on the new model containing more fuel rods. The next will be a research of the effect of deposits at the fuel rod wall on the heat transfer. The experience gained during the measurements allows us to better understand the very complex physical phenomenon of the heat transfer crisis on the specific case of the fuel rod model. We will also use them in the investigation of the heat transfer crisis in the large water loop at the Škoda JS a.s.

References

1. SEDLÁČEK, J., ERET, P., MATAS, R. BRABEC, B. Úpravy a vývoj experimentálního zařízení pro výzkum přestupu tepla při tlaku blízkém atmosférickému. Technická zpráva NTC-VYZ-21-065, Plzeň, 2021.
2. MATAS, J., JANOUŠ, J., KLAVÍK, P., SEDLÁČEK, J., MATAS, R. Odborná zpráva o řešení projektu TAČR THETA II, č. TK02020033, za období 2021. Technický document Ae22104/Dok Rev.0, Plzeň, 2022.
3. LÁVIČKA, D., KNAPP, Y., POLANSKÝ, J. Investigation of thermal-hydraulic field in the annular channel around the heated wall of the fuel rod. IMECE2013-64174. San Diego, ASME, 2013.
4. KLAVÍK, P. Časoprostorová analýza nestacionárních polí. Teze disertační práce. Plzeň: Západočeská univerzita v Plzni, Katedra energetických strojů a zařízení, 2021.
5. KLAVÍK, P. Fyzikální modelování proudění v palivovém souboru v aktivní zóně jaderného reaktoru . Plzeň: Západočeská univerzita v Plzni, Katedra energetických strojů a zařízení, 2017.
6. KLÍMA, T. CFD modelování proudění v palivovém souboru v aktivní zóně jaderného reaktoru. Plzeň: Západočeská univerzita v Plzni, Katedra energetických strojů a zařízení, 2017.
7. Styrikovich, M., A., Polonsky, V., S., Tsiklauri, G., V. Two-phase cooling and corrosion in nuclear power plants. High Temperature Institute of the USSR Academy of Sciences, Moscow, English-Edition editor Hewitt, G., F. Harwell, 1987. ISBN 3-540-18106-7

Acknowledgments

The research has been supported by the n.:TK02020033 - Experimental and computational critical heat flux identification of small power output reactor (SMR) fuel rods granted by Technology Agency of Czech Republic.

TWO PHASE FLOW BOILING SIMULATIONS OF DEBORA EXPERIMENTS USING EULERIAN CFD APPROACH

Daniel VLČEK[1], Yohei SATO[2]

[1]Czech Technical University in Prague; State Office for Nuclear Safety, Czech Republic
[2] Paul Scherrer Institute, Switzerland

Thermal hydraulic analyses of the Light Water Reactors are being conducted for decades mainly with 1D system or subchannel codes in which the governing equations are closed usually with empirical correlations based on experimental data. The codes have been thoroughly tested and it has been confirmed that they are robust, reliable and quick. On the other hand, the empirical correlations have usually limited range of applicability. Therefore, current trends and growing computing power are towards multidimensional approaches relying more on physical solutions rather than on expensive experimental data for such analyses.

For this purpose, Computational Fluid Dynamics (CFD) method can be used. With this method, the results can be obtained in much greater detail, but with a cost of longer computational time and with a lost of straightforward setup of 1D codes. During the last twenty years, various CFD codes have been developing continuously and now it is possible to choose among many implemented models. However, the choice of the model depends on trial-and-error and the use of the most complex models is not always the best solution.

Two phase flow boiling simulations of DEBORA experiments using Eulerian CFD approach

Daniel Vlček[1] and Yohei Sato[2]

1) Czech Technical University in Prague; State Office for Nuclear Safety – **daniel.vlcek@sujb.cz** 2) Paul Scherrer Institut

Introduction and motivation

- Thermal hydraulic analyses of the Light Water Reactors are being conducted for decades mainly with 1D system or subchannel codes in which the governing equations are closed usually with empirical correlations based on experimental data. The codes have been thoroughly tested and it has been confirmed that they are robust, reliable and quick. On the other hand, the empirical correlations have usually limited range of applicability. Therefore, current trends and growing computing power are towards multidimensional approaches relying more on physical solutions rather than on expensive experimental data for such analyses.
- For this purpose, Computational Fluid Dynamics (CFD) method can be used. With this method, the results can be obtained in much greater detail, but with a cost of longer computational time and with a lost of straightforward setup of 1D codes. During the last twenty years, various CFD codes have been developing continuously and now it is possible to choose among many implemented models. However, the choice of the model depends on trial-and-error and the use of the most complex models is not always the best solution.

Figure 1

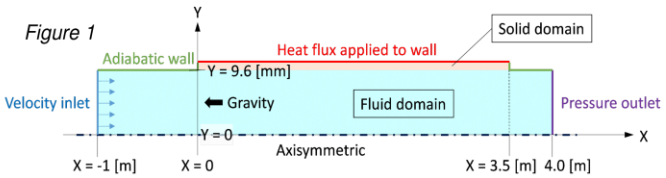

- In this work, we propose two modified zero closure models, based on the original zero closure model [1], and the validation of the DEBORA experiments is presented. The comparison with the selected cases are shown here together with the description of the simulation setup.
- The DEBORA experiments were simulated many times (e. g. Krepper [2] and Vyskocil [3]), although the simulation results comply only with the cases where the void fraction increases near the heated wall. If cases with maximum void fraction in the centre are selected, the models fail to predict the decreasing vapor void fraction.

Description of the model

- Two combinations of closure models were evaluated, both employing the concept of zero closure model, which focuses on a simple and robust implementation of the key two-phase flow boiling physics mechanisms.
- The models were implemented into ANSYS Fluent using Eulerian multiphase approach. The k-ω SST (mixture) turbulence model was used together with Sato's bubble induced turbulence model.
- 2. model uses MUSIG Population Balance Model (PBM) with Luo and Svendsen model for breakage with factor 0.5 and Prince and Blanch model for coalescence with factor 0.2. Twenty uniform groups are chosen from minimum diameter of 0.01 mm to maximum diameter of 3.5 mm.

Closure equation	1. Model	2. Model
Interfacial area concentration (IAC)	Transport with Ishii-Kim source terms	Algebraic particle
Bubble size	Sauter diameter from IAC	Population balance model
Wall boiling model	Classic RPI	Non-equilibrium RPI
Nucleation site density	Kocamustafaogullari-Ishii	Li [4]
Bubble departure diameter	Kocamustafaogullari-Ishii	**Modified Tolubinsky-Konstanchuk** (1)
Bubble departure frequency	Cole	Cole
Quenching correction	Off	On
Drag force	Ishii-Zuber	Ishii-Zuber
Lift force	**Modified Yoon (C_{+}=10)**	**Modified Yoon (C_{+}=5;3)** (2)
Turbulent dispersion force	Burns	Burns
Wall lubrication force	Constant coef. = 1	Constant coef = 1
Virtual mass force	Not used	Not used
Mass transfer model – two resistance	Chen-Meyinger Nu=2	Ranz-Marshall Zero-resistance

$$D_w = \min\left(0.0014, 5e-5\cdot\exp\left[\frac{\Delta T_{sub}}{45.0}\right]\right) \quad (1) \qquad C_l = \begin{cases} 0.025 * C_{+} & \alpha_g \le 0.25 \\ -0.025 * C_{-} & 0.25 < \alpha_g \end{cases} \quad (2)$$

Comparison with experimental data

- Steady state simulations on the 2D axisymmetric coordinate system were performed with the boundary conditions depicted in Fig. 1. Based on the mesh sensitivity analysis result, the mesh with 40 × 2000 nodes was used. The spatial discretisation scheme was set to at least second-order accuracy.
- Three cases of DEBORA simulations, i. e. subcooled convective boiling flow of refrigerant R12 in vertical pipe [5], are shown here as the representatives.

Case	G (kg.m^{-2}.s^{-1})	q (kW.m^{-2})	P_{out}(bar)	T_{in} (°C)
1	2030.0	69.07	14.59	31.2
2	2022.9	69.07	14.59	39.7
3	2024.1	69.07	14.59	44.2

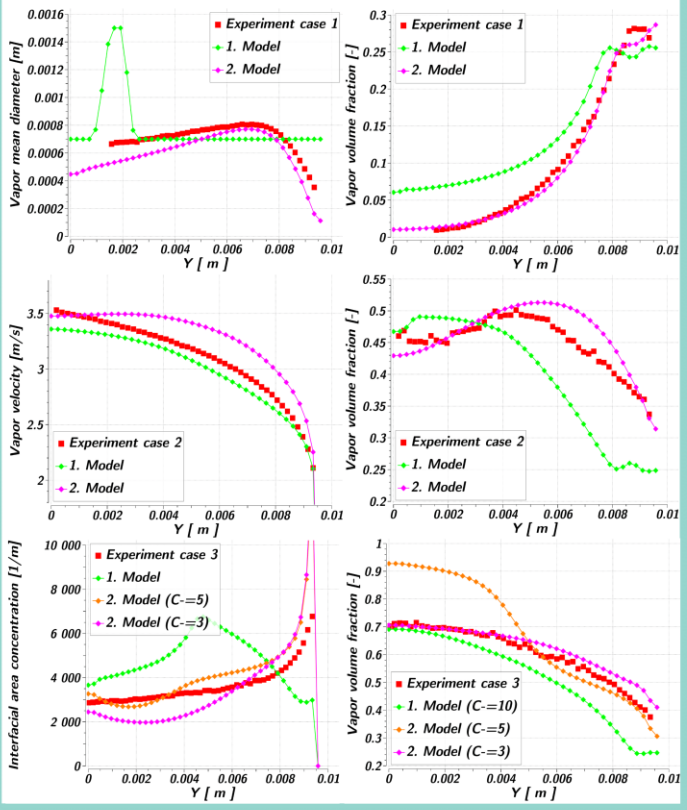

Conclusion

- Results imply that for good representation of vapor bubble diameter and IAC the population balance model is necessary.
- Both models show great tendency of void fraction captured mainly by modified lift force model. 2. model perfectly predicts the void fraction due to better solution of bubble size. 1. model underpredicts the total amount of void.
- Velocities calculated by both models comply with experimental results with acceptable deviations.
- The final model with PBM is still prone to tuning of some coefficients (Coalescence and breakage factors, constant in bubble departure diameter model, lift force coefficients) which influence the results greatly, thus creation of universal model is necessary, however, these results help to understand the subcooled flow boiling behaviour.

Acknowledgements and references

This work is supported by IAEA project number CZR0010 and by Czech Technical University in Prague with its Student grant contest project with the code SGS20/187/OHK4/3T/14. The support of State Office for Nuclear Safety is greatly acknowledged.

[1] Baglietto, E. and Christon, M., "Demonstration and assessment of advanced modeling capabilities for multiphase flow with sub-cooled boiling," CASL-U-2013-0181-001, (2013).
[2] Krepper, E. and Rzehak, R., "CFD for subcooled flow boiling," Nuclear Engineering and Design, 241(9), pp. 3851–3866, (2011).
[3] L. Vyskocil and J. Macek, "Boiling flow simulation in neptune-cfd and fluent codes," NURESIM, (Rez, Czech republic), pp. 1-13, (2010).
[4] Q. Li, Y. Jiao, M. Avramova, P. Chen et al. "Development, verification and application of a new model for active nucleation site density in boiling systems," Nuclear Engineering and Design, vol. 328, pp. 1-9, (2018).
[5] J. Garnier, E. Manon, and G. Cubizolles, " Local measurements on flow boiling of refrigerant 12 in a vertical tube," Multiphase Science and Technology, vol. 13, pp. 1-111, (2001).

THE NEW CONCEPT OF NEUTRON ABSORBERS PLACED DIRECTLY WITHIN SPENT NUCLEAR FUEL

Jiří ZÁVORKA[1], Martin LOVECKÝ[1], Jana JIŘÍČKOVÁ[1] and Radek ŠKODA[1,2]

[1]University of West Bohemia, Pilsen, Czech Republic
[2]Czech Technical University in Prague, Prague, Czech Republic

A unique solution presented in this poster is based on special fixed neutron absorbers placed directly within the nuclear fuel assembly. The absorbers are permanently connected in specially designed tubes, which decreases system reactivity more efficiently than absorber sheets between the assemblies. This solution is more efficient than absorber tubes, even with a neutron flux trap. Hence, it allows significant basket design changes, e.g., lowering boron content in steal or decreasing fuel assembly pitch in the basket resulting in lower cask wall diameter and lower total cask mass.

NUCLEAR DAYS 2022 in Pilsen 14. 9. - 19. 10.

The New Concept of Neutron Absorbers Placed Directly within Spent Nuclear Fuel

Jiří Závorka[1], Martin Lovecký[1], Jana Jiříčková[1] and Radek Škoda[1,2]

[1]University of West Bohemia, Pilsen, Czech Republic, e-mail: zavorka@fel.zcu.cz

[2]Czech Technical University, Prague, Czech Republic

Introduction

A unique solution presented in this poster is based on special fixed neutron absorbers placed directly within the nuclear fuel assembly. The absorbers are permanently connected in specially designed tubes, whitch decreases system reactivity more efficiently than absorber sheets between the assemblies. This solution is more efficient than absorber tubes, even with a neutron flux trap. Hence, it allows significant basket design changes, e.g., lowering boron content in steal or decreasing fuel assembly pitch in the basket resulting in lower cask wall diameter and lower total cask mass.

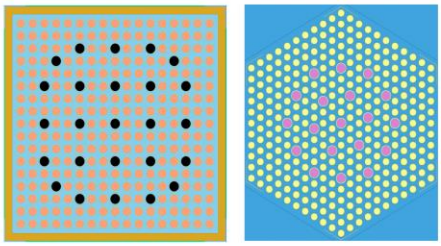

Fig. 1: Neutron fixed absorber concept in nuclear fuel, PWR fuel type (black color), WWER fuel type (purple color).

Concept

Legislative and criticality safety margins are commonly achieved by placing neutron absorbers in the cask basket design. Currently, boron content in steel is exclusively used in transport and storage absorber components as the absorber material. Mechanical and chemical properties of absorbing light boron nuclei allow adding boron directly to basket tubes material or in extra sheets between the tubes. Nevertheless, with higher fuel enrichment and limit on boron content in steel or alloys, criticality safety criteria are currently not easily met. The presented solution is a unique approach based on placing neutron absorbers in the most effective location.

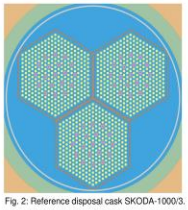

Fig. 2: Reference disposal cask SKODA-1000/3.

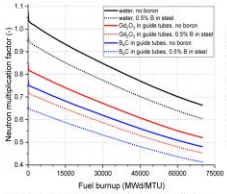

Fig. 3: Results for final disposal cask in wet conditions.

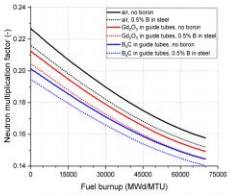

Fig. 4: Results for final disposal cask in dry conditions.

A summary of the fixed absorber concept for spent fuel transport, storage and disposal is:

- The decrease of the reactivity in the disposal cask in both wet and dry conditions was compared to standard approach with absorber tubes. The resulting effect is the possibility to reduce the cost of the cask, for example by reducing the fuel assembly pitch that leads to reduced cask dimensions.
- Tested suitable materials are B_4C or Gd_2O_3.
- The concept decreases neutron fluence by 5 % due to subcritical multiplication. Consequently, the associated dose is decreased.
- The possibility of replacing expensive borated steel within the cask construction. Cask basket redesign would allow smaller cask wall diameter and lower wall mass.

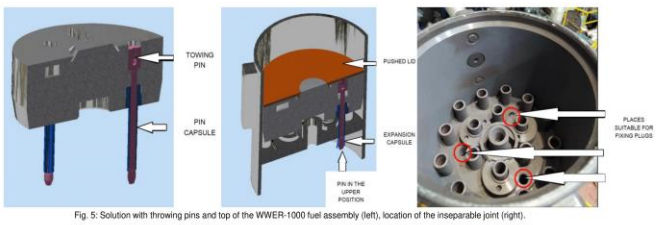

Fig. 5: Solution with throwing pins and top of the WWER-1000 fuel assembly (left), location of the inseparable joint (right).

Experiment part

The basic premise of the whole concept is the inseparability of the fixed neutron absorber. This practical part of the research focused on the development of a fixed connection between absorber and fuel assembly. Obviously, the concept is suitable only for selected fuel assembly types. For our new prototype, we focused on the WWER-1000 fuel assembly.

In this variant, it is assumed that the plug of the fuel assembly will be secured with three towing pins. The pins will be subjected to tensile stress when securing the plug. After pulling the pins into the pin capsule, the ends of the pin will expand to the wall of pin capsule and become fixed. The ends of the locking pins will be subjected to tensile stress see the solution in Figures above.

Verification part

This part of selecting elements is essential background for the following research. Categories I. and II. were used for an experimental part as input data for a prototype. The following requirements play a crucial role in future prototype production:

- Physical (melting point, density, chemical resistance etc.) properties of selected elements.
- Price of selected elements. The final product should also make sense from an economic point of view.

The following materials were chosen:

Gd_2O_3 powder in a stainless steel tube.

Sm_2O_3 powder in a stainless steel tube.

Fig. 6: Sm_2O_3 absorber in a stainless steel tube.

The objective of the experimental verification of the neutron absorber for VVER-1000 fuel at LR-0 is to determine the critical level for 4 cases:

1. Reference: neutron field with 7x FA (6x 3.30% and 1x 1.60% U-235), low enriched fuel in the central position will be ready for insertion of absorbers.
2. Central FA with inserted 6x Sm_2O_3 absorbers into the inner row of guide tubes of the central PS.

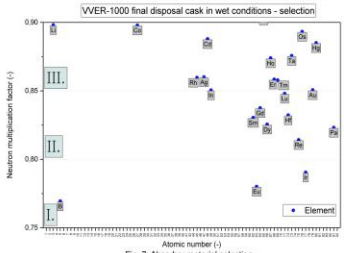

Fig. 7: Absorber material selection.

3. Central FA with inserted 6x Gd_2O_3 absorbers into the inner row of guide tubes of the central PS.
4. Final case, 6x Gd_2O_3 absorbers into the inner row and 12x Sm_2O_3 into the outer row.

Table 1: Experiment verification of neutron absorbers in the LR-0 reactor.

Case [-]	1	2	3	4
Critical water level [cm]	34.63	37.39	37.41	42.63
Δ k-eff (exp. – calc.) [pcm]	22	6	-28	-3
Number of Gd abs. [-]	0	0	6	6
Number of Sm abs. [-]	0	6	0	12
Absorber weight [pcm]	0	1481	1497	3866

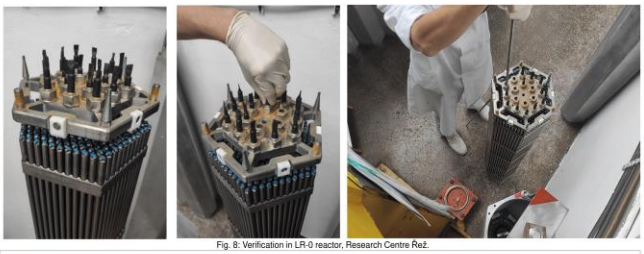

Fig. 8: Verification in LR-0 reactor, Research Centre Řež.

Conclusions

Based on complex studies, it was proven that this concept brings:

- Improved safety – decrease in cask reactivity with the possibility to remove the requirement to use burnup credit methodology, criticality safety limits are met even with the fresh fuel.
- Better economics – Due to improved neutronic properties, system/facility redesign is allowed, for example: design with no stainless steel tubes between fuel assemblies in the final disposal casks and significantly reduced cask wall inner diameter (cheap but high-quality materials were used, including a simple mechanical connection to fuel assembly).
- It is possible to lower the pitch between fuel assemblies. E.g., for the GBC-32 benchmark cask, it reduces 7.65% wall mass.
- The prototype was prepared and verified in the LR-0 reactor.

Acknowledgments

R&D has been funded by TK02010102 Optimization of Dry Storage for Spent Nuclear Fuel.

References

[1] ZÁVORKA, J., LOVECKÝ, M., JIŘIČKOVÁ, J., ŠKODA, R., Enhanced nuclear safety of spent fuel, In Proceedings of the 27th International Conference on Nuclear Engineering (ICONE27), New York: American Society of Mechanical Engineers (ASME), 2019, s. 1-4., ISBN 978-4-88898-305-1.

[2] LOVECKÝ, M., ZÁVORKA, J., ŠKODA, R., Neutron absorber concept in spent fuel casks aiming at improved nuclear safety and better economics, In Proceedings of the 19th International Symposium on the Packaging and Transportation of Radioactive Materials (PATRAM 2019), New Jersey: Institute of Nuclear Materials Management, 2019.

[3] ZÁVORKA, J., LOVECKÝ, M., JIŘIČKOVÁ, J., ŠKODA, R., New neutron absorber in spent fuel casks aiming at improved nuclear safety and better economics, 2021 International Congress on Advances in Nuclear Power Plants (ICAPP 2021), Abu Dhabi, UAE, 2021.

[4] LOVECKÝ, M., ZÁVORKA, J., JIŘIČKOVÁ, J., ŠKODA, R., Criticality safety analysis of GBC-32 spent fuel cask with improved neutron absorber concept, In Proceedings of the PHYSOR 2020, La Grande Park: American Nuclear Society, 2020, p. 1-8., ISBN 978-1-5272-6447-2.

[5] LOVECKÝ, M., ZÁVORKA, J., JIŘIČKOVÁ, J., ŠKODA, R., Increasing efficiency of nuclear fuel using burnable absorbers, Progress in Nuclear Energy, 2020, edition 118, January 2020, p. 1-12., ISSN: 0149-1970.

[6] LOVECKÝ, M., ZÁVORKA, J., JIŘIČKOVÁ, J., ŠKODA, R., Neutron absorber for VVER-1000 final disposal cask, In Proceedings: 29th International Conference Nuclear Energy for New Europe (NENE 2020), Ljubljana: Nuclear Society of Slovenia, 2020, p. 1502.1-1502.8, ISBN 978-961-6207-49-2.

ACKNOWLEDGMENT

This event was supported by the Student Scientific Conference 2022 (SVK project) "*Conference of Nuclear Days 2022"* of the University of West Bohemia in Pilsen. Project number is SVK1-2022-003.